

1 **Impact of Intercontinental Pollution Transport on North American Ozone Air Pollution:**
2 **An HTAP Phase 2 Multi-model Study**

3
4 Min Huang^{1,2}, Gregory R. Carmichael³, R. Bradley Pierce⁴, Duseong S. Jo⁵, Rokjin J. Park⁵,
5 Johannes Flemming⁶, Louisa K. Emmons⁷, Kevin W. Bowman⁸, Daven K. Henze⁹, Yanko Davila⁹,
6 Kengo Sudo¹⁰, Jan Eiof Jonson¹¹, Marianne Tronstad Lund¹², Greet Janssens-Maenhout¹³,
7 Frank J. Dentener¹³, Terry J. Keating¹⁴, Hilke Oetjen^{8,*}, Vivienne H. Payne⁸

8
9 ¹George Mason University, Fairfax, VA, USA

10 ²University of Maryland, College Park, MD, USA

11 ³University of Iowa, Iowa City, IA, USA

12 ⁴NOAA National Environmental Satellite, Data, and Information Service, Madison, WI, USA

13 ⁵Seoul National University, Seoul, Korea

14 ⁶European Center for Medium range Weather Forecasting, Reading, UK

15 ⁷National Center for Atmospheric Research, Boulder, CO, USA

16 ⁸Jet Propulsion Laboratory, California Institute of Technology, Pasadena, CA, USA

17 ⁹University of Colorado-Boulder, Boulder, CO, USA

18 ¹⁰Nagoya University, Furocho, Chigusa-ku, Nagoya, Japan

19 ¹¹Norwegian Meteorological Institute, Oslo, Norway

20 ¹²Center for International Climate and Environmental Research, Oslo, Norway

21 ¹³European Commission, Joint Research Center, Ispra, Italy

22 ¹⁴US Environmental Protection Agency, Washington, DC, USA

23 *Now at: University of Leicester, Leicester, UK

24
25 *Correspondence to:* Min Huang (mhuang10@gmu.edu)

26 **Abstract**

27
28 The recent update on the US National Ambient Air Quality Standards of the ground-level
29 ozone (O₃) can benefit from a better understanding of its source contributions in different US
30 regions during recent years. In the Hemispheric Transport of Air Pollution experiment Phase 1
31 (HTAP1), various global models were used to determine the O₃ source-receptor relationships
32 among three continents in the Northern Hemisphere in 2001. In support of the HTAP Phase 2
33 (HTAP2) experiment that studies more recent years and involves higher-resolution global models
34 and regional models' participation, we conduct a number of regional scale Sulfur Transport and
35 dEposition Model (STEM) air quality base and sensitivity simulations over North America during
36 May-June 2010. STEM's top and lateral chemical boundary conditions were downscaled from
37 three global chemical transport models' (i.e., GEOS-Chem, RAQMS, and ECMWF C-IFS) base
38 and sensitivity simulations in which the East Asian (EAS) anthropogenic emissions were reduced
39 by 20%. The mean differences between STEM surface O₃ sensitivities to the emission changes
40 and its corresponding boundary condition model's are smaller than those among its boundary
41 condition models, in terms of the regional/period mean (<10%) and the spatial distributions. An
42 additional STEM simulation was performed in which the boundary conditions were downscaled
43 from a RAQMS simulation without EAS anthropogenic emissions. The scalability of O₃
44 sensitivities to the size of the emission perturbation is spatially varying, and the full (i.e., based on
45 100% emission perturbation) source contribution obtained from linearly scaling the North
46 American mean O₃ sensitivities to a 20% reduction in the EAS anthropogenic emissions may be
47 underestimated by at least 10%. The three boundary condition models' mean O₃ sensitivities to
48 the 20% EAS emission perturbations are ~8% (May-June 2010)/~11% (2010 annual) lower than
49 those estimated by eight global models, and the multi-model ensemble estimates are higher than
50 the HTAP1 reported 2001 conditions. GEOS-Chem sensitivities indicate that the EAS
51 anthropogenic NO_x emissions matter more than the other EAS O₃ precursors to the North
52 American O₃, qualitatively consistent with previous adjoint sensitivity calculations.

53 In addition to the analyses on large spatial/temporal scales relative to the HTAP1, we also
54 show results on subcontinental- and event-scale that are more relevant to the US air quality
55 management. The EAS pollution impacts are weaker during observed O₃ exceedances than on all
56 days in most US regions except over some high terrain western US rural/remote areas. Satellite O₃
57 (TES, JPL-IASI, and AIRS) and carbon monoxide (TES and AIRS) products, along with surface
58 measurements and model calculations, show that during certain episodes stratospheric O₃
59 intrusions and the transported EAS pollution influenced O₃ in the western and the eastern US
60 differently. Free-running (i.e., without chemical data assimilation) global models underpredicted
61 the transported background O₃ during these episodes, posing difficulties for STEM to accurately
62 simulate the surface O₃ and its source contribution. Although we effectively improved the modeled
63 O₃ by incorporating satellite O₃ (OMI and MLS) and evaluated the quality of the HTAP2 emission
64 inventory with the KNMI OMI nitrogen dioxide, using observations to evaluate and improve O₃
65 source attribution still remains to be further explored.

1. Introduction

Tropospheric ozone (O_3), a short-lived trace gas with a lifetime ranging from hours in the boundary layer to weeks in the free troposphere, affects tropospheric chemistry, harms human and ecosystem health, and induces climate change on local, regional and global scales (Jerrett et al., 2009; Smith et al., 2009; Anenberg et al., 2010; Mauzerall and Wang, 2001; Avnery et al., 2011a, b; Shindell et al., 2009, 2013; Bowman and Henze, 2012; Stevenson et al., 2006, 2013; Monks et al., 2015). It has been recognized that the uneven distributions of tropospheric O_3 can be attributed to the stratosphere as well as local, regional and distant emission sources, through complicated processes that occur on synoptic, meso- and micro-scales (Task Force on Hemispheric Transport of Air Pollution (HTAP), 2010; National Research Council (NRC), 2009; Maas and Grennfelt, 2016). The mitigation of O_3 's climate and health impacts would benefit from efforts to control the emissions of its precursors from the various emission sources (United Nations Environment Programme (UNEP) and World Meteorological Organization (WMO), 2011), such as nitrogen oxides (NO_x), carbon monoxide (CO), methane (CH_4), and non-methane volatile organic compounds (NMVOCs).

Ground-level O_3 is one of the six criteria air pollutants regulated by the US Environmental Protection Agency (EPA), and the US National Ambient Air Quality Standards (NAAQS) has recently been lowered to 70 ppbv to better protect Americans' health and the environment. Issues regarding making accurate estimates of the total O_3 as well as the background O_3 level (defined as the concentration that is not affected by recent locally-emitted or produced anthropogenic pollution) (e.g., McDonald-Buller et al., 2011; Zhang et al., 2011; Fiore et al., 2014; Huang et al., 2015), have been recently discussed as part of the implementation of the new US O_3 standard (US EPA, 2016a, b). This includes assessing the impacts of various components of the background O_3 , such as stratospheric O_3 , local natural sources such as biogenic, lightning and wildfire emissions, as well as the long-range transport (LRT) of pollution. The impact of the trans-Pacific pollution transport on US air quality has been evaluated in numerous studies over the past decades (e.g., Fiore et al., 2009; Reidmiller et al., 2009; Zhang et al., 2008, 2009; Huang et al., 2010, 2013a; Lin et al., 2012a, 2015, 2016; US EPA, 2016a). It has been found that the increasing trends of pollution in the upwind continents, especially the populated East Asia (e.g., Zhang et al., 2014; Susaya et al., 2013; Wang et al., 2012), may partially offset the US air quality improvements in recent decades due to the regional and local emission controls (e.g., Jacob et al., 1999; Verstraeten et al., 2015; Ambrose et al., 2011; Wigder et al., 2013; Cooper et al., 2010; Parrish et al., 2009, 2012; Gratz et al., 2014). A better understanding of the processes that determine the O_3 pollution levels, as well as an improved capability of attributing the air pollution to nearby or distant sources is needed to assist with designing and implementing effective local emission control strategies to comply with the tighter air quality standards.

Chemical transport models are often used to reproduce and attribute the observed O_3 levels, including assessing the impacts of the internationally transported O_3 on the US air quality. In the HTAP modeling experiment Phase 1 (HTAP1), various global models with horizontal resolutions ranging from $1^\circ \times 1^\circ$ to $5^\circ \times 5^\circ$, only around half of which are finer than $3^\circ \times 3^\circ$, were used to determine the O_3 source-receptor (SR) relationships among three continents in the Northern Hemisphere in 2001 (Chapter 4 in HTAP, 2010). The global model based SR relationships in HTAP1 determined using the emission perturbation approach (i.e., calculating the changes of O_3

112 at the receptor regions in response to a 20% reduction in the emission inputs in a given source
113 region) were reported as either monthly 24h mean values or policy-relevant metrics such as the
114 maximum daily 8h average (MDA8) for the US (e.g., Fiore et al., 2009; Reidmiller et al., 2009).
115 Large intermodel diversity was found in the simulated total O₃ and the intercontinentally
116 transported pollution for the chosen SR pairs in the northern midlatitudes, indicating the challenges
117 with model simulations to accurately represent the key atmospheric processes. Multi-model mean
118 results were the foci of in these studies with the assumption that this approach can reduce the
119 uncertainty from the single model estimates for monthly or seasonal means. “Ensemble” model
120 analyses have been suggested by some US stakeholders as one of the methods for helping with the
121 characterization of the background O₃ components (US EPA, 2016b). Although the multi-model
122 approach can help identify some of the weaknesses of the individual models and may produce
123 more reliable estimates, it is necessary to well understand the uncertainties inherent in using the
124 same set of anthropogenic emissions in all these model simulations. Satellite observations over the
125 regions with limited in-situ measurements such as the East Asia can be particularly helpful for
126 quantifying such uncertainties.

127
128 The 20% emission perturbation in the HTAP1 modeling experiment was chosen to produce
129 a sizeable (i.e., larger than numerical noise) and realistic impact, but small enough in the assumed
130 near-linear atmospheric chemistry regime. The scalability of the modeled O₃ sensitivities to the
131 size of the emission perturbations has been assessed on continental scale (Wu et al., 2009; Fiore et
132 al., 2009; HTAP, 2010; Wild et al., 2012; Emmons et al., 2012). The receptor O₃ responses to the
133 source-region emission perturbations are found to be fairly linear within ~50% of the perturbations.
134 However, due to the chemical non-linearity, the full source contribution obtained by linearly
135 scaling the receptor regional mean O₃ sensitivity to the 20% reduction in the source region
136 emissions may be underestimated, and the scalability depended on seasons and the perturbed
137 emission species. Huang et al. (2013b) investigated the scalability of the O₃ sensitivity between
138 the southern California-US intermountain west SR pair for May 2010, in which study the southern
139 California anthropogenic emissions were perturbed by multiple amounts of +50%, -50%, -100%.
140 They reported that the scalability of the O₃ sensitivities changed with the distance from the source
141 regions. Further analyses on the scalability of these modeled O₃ sensitivities during recent years
142 especially for the East Asia-NAM SR pair, as well as their spatial variability, are still needed.
143 Furthermore, results generated using the emission perturbation approach need to be compared with
144 those based on the other methods (e.g., tagged tracers, adjoint sensitivity).

145
146 Previous studies have demonstrated the advantages of high resolution chemical transport
147 modeling for understanding SR relationships (e.g., Lin et al., 2010 for Europe and the East Asia;
148 Lin et al., 2012a; Huang et al., 2010, 2013a for Asia and NAM). Using observations (satellite,
149 sondes, aircraft) along with single model simulations, a few studies have reported that the US O₃
150 sensitivities to extra-regional sources is time- and region-dependent (e.g., Lin et al., 2012a, b;
151 Langford et al., 2011; Ott et al., 2016), and therefore the necessity of evaluating the extra-regional
152 source impacts on event scale has been emphasized in these studies as well as in US EPA (2016a,
153 b). The HTAP Phase 2 (HTAP2) multi-model experiment, initiated in 2012, is designed to advance
154 the understanding of the impact of intercontinental pollution transport during more recent years
155 (i.e., 2008-2010) involving a number of global and regional models’ participation (Galmarini et
156 al., 2017; Koffi et al., 2016). The regional models are anticipated to help connect the analyses over
157 global and regional scales and enable discussions on small spatial (e.g., subcontinental) and

158 temporal scales (i.e., event based analyses). The use of satellite products for identifying the
159 transport events as well as for quantitative model evaluation is also encouraged in the work plan.
160 The HTAP2 modeling experiment was sequentially conducted in two steps. First, similar to the
161 HTAP1 experiment, a group of global models with different resolutions conducted base and
162 emission perturbation sensitivity simulations to determine the pollutants' SR relationships. All
163 models in their base simulations used the same set of harmonized sector-based global
164 anthropogenic emissions developed specifically for the HTAP2 modeling experiment (Janssens-
165 Maenhout et al., 2015). Most of these global models recorded only key chemical species from their
166 base and sensitivity simulations in varied temporal frequencies. Several global models saved the
167 three-dimensional (3D) chemical fields of more species with a 3- or 6-hour interval, which are
168 suitable for being used as regional models' chemical boundary conditions. In the second step,
169 regional models conducted base and sensitivity simulations to analyze the pollutants' SR
170 relationships in greater detail. The regional model simulations used the same set of anthropogenic
171 emissions as the global models within their simulation domains, and the chemical boundary
172 conditions in these regional simulations were downscaled from the base and sensitivity simulations
173 from the selected boundary condition model outputs. For regional simulations over the North
174 America and Europe, boundary conditions were mostly taken from a single model such as the
175 ECMWF C-IFS or GEOS-Chem.

176
177 This study aims to address: 1) comparing the differences in O₃ sensitivities generated from
178 the HTAP2 and HTAP1 experiments, which could help address how the LRT impacts on NAM
179 changed through time; 2) how the refined modeling experiment design in HTAP2 can help advance
180 our understanding of the LRT impacts on NAM, particularly the involvement of regional models
181 and the inclusion of small spatial/temporal scale analysis during high O₃ episodes that are more
182 relevant to air quality management; 3) the usefulness of satellite observations for better
183 understanding the sources of uncertainties in the modeled total O₃ (e.g., from the emission and
184 regional models' boundary condition inputs) as well as for reducing the uncertainties in some of
185 these model inputs via chemical data assimilation. We performed a number of regional scale
186 STEM (Sulfur Transport and dEposition Model) base and sensitivity simulations over the NAM
187 during May-June 2010, during which period strong trans-Pacific pollution transport were shown
188 to episodically impact the US (Lin et al., 2012a). Extending the HTAP2 regional simulations' basic
189 setup, the STEM top and lateral chemical boundary conditions were downscaled from three global
190 models' (i.e., the Seoul National University (SNU) GEOS-Chem, RAQMS, and the ECMWF C-
191 IFS) base and sensitivity simulations in which the East Asian anthropogenic emissions were
192 reduced. The STEM surface O₃ sensitivities over the NAM region based on different boundary
193 condition models were inter-compared, in terms of the regional averages and the spatial patterns
194 on monthly basis and during a selected event identified by satellite O₃ and CO products. These
195 were also compared with the sensitivities estimated by their corresponding boundary condition
196 models as well as all HTAP2 participating global models and the results from HTAP1.

197 198 **2. Methods**

199 *2.1. Anthropogenic emission inputs*

200
201 Identical anthropogenic emissions were used in all global and regional chemical transport
202 models' base and sensitivity simulations. This monthly-varying harmonized sectoral (i.e., power,
203 industry, transportation, residential, shipping, aircraft, agriculture) emission inventory was

204 provided on a gridded $0.1^\circ \times 0.1^\circ$ resolution for the years of 2008 and 2010, by compiling the
205 officially reported emissions at the national scale (Janssens-Maenhout et al., 2015;
206 http://edgar.jrc.ec.europa.eu/htap_v2). The temporal profiles for developing the monthly-varying
207 emissions differ by region and sector. The amount of emissions of key O₃ precursors (CO, NO_x,
208 NMVOCs) from both years are summarized in Table S1 for the four major emissions sectors, over
209 the NAM (US+Canada, based on data from the US EPA and the Environmental Canada, which
210 shows lower emissions from the previous years as also discussed in Pouliot et al., 2015), MICS-
211 Asia regions (south, southeast, and east Asia, based on country inventory for China and from the
212 Clean Air Policy Support System and the Regional Emission inventory in ASia 2.1, more
213 information also in Li et al., 2017), and for over the world. For all of these species, global total
214 emissions in 2008 and 2010 are similar. The NO_x, NMVOC, and CO emissions decreased from
215 2008 to 2010 over the NAM by 10.7%, 9.4%, and 15.7%, respectively. In 2008, NAM NO_x,
216 NMVOC and CO contributed to 18.0%, 11.7% and 11.9% of the global total, respectively, and in
217 2010, these contributions became 15.8%, 10.5% and 10.2%. For 2010, the transportation sector
218 contributed more than the other sectors to NAM anthropogenic NO_x and CO emissions; industrial
219 sector contributed more than the other sectors to NMVOCs emissions. Over East Asian countries,
220 these emissions are ~2-5 times higher than the US emissions, and the NO_x, NMVOC and CO
221 emissions increased over Asia by 7.3%, 7.2% and 1.0%, with the dominant emission sectors in
222 2010 of transportation, industry, and residential, respectively. For both years, the emissions over
223 the MICS-Asia regions contribute to over 40% of the global emissions. For these key O₃ precursors,
224 the East Asian countries contribute to 45% (NMVOCs)-70% (NO_x) of the emissions in the MICS-
225 Asia domain in both years, and the south Asian countries contribute to ~22% (NO_x)-34%
226 (NMVOCs) of the MICS-Asia emissions. The uncertainty of the emission estimates differs by
227 emission sector and species: i.e., the emissions from large-scale combustion sources (e.g., NO_x
228 and CO from power and industry sectors) are less uncertain than those from small-scale and
229 scattered sources (e.g., CO and NMVOCs from transportation and residential sources). Non-
230 anthropogenic emission inputs used in different models' simulations may differ, and their impacts
231 on the modeled total O₃ and the SR relationships will be compared in detail in future studies.

232

233 2.2. *Region definitions for the SR study and the model base and sensitivity simulations*

234 2.2.1. Base and 20% emission perturbation simulations from global and regional models

235 The HTAP2 simulations from eight global models, used in this study, are listed in Table
236 1a, including the relevant references. Horizontal and vertical resolutions of these models range
237 from finer than 1° to coarser than 2.5° , and from 20 to 60 layers, respectively. Overall these
238 resolutions are higher than the HTAP1 participating models'. Figure 1 defines the source regions
239 used in the HTAP2 SR relationship study and we will focus in this study on assessing the East
240 Asia (EAS), S Asia (SAS), Europe (EUR), and non-NAM anthropogenic source (interchangeable
241 in this paper with "(all) foreign") impacts on the NAM O₃ levels in 2010. Specifically, each model
242 performed a base simulation and a number of sensitivity simulations in which the original HTAP2
243 anthropogenic emissions for all species and sectors in a defined source region were perturbed by
244 a certain amount (referring to 20% as in most cases) and these cases are defined in Table 1a-b as
245 **source region*ALL(*perturbation*)*, where "ALL" refers to "all species and sectors", consistent
246 with HTAP1 and HTAP2's naming convention. The O₃ differences $R(O_3, *source\ region*,$
247 **perturbation*)* over the NAM were then calculated between each model's base and sensitivity
248 simulations:

249

250 $R(O_3, EAS, 20\%) = BASE O_3 - EASALL(-20\%) O_3$ (1a)

251 $R(O_3, SAS, 20\%) = BASE O_3 - SASALL(-20\%) O_3$ (1b)

252 $R(O_3, EUR, 20\%) = BASE O_3 - EURALL(-20\%) O_3$ (1c)

253 $R(O_3, non-NAM, 20\%) = NAMALL(-20\%) O_3 - GLOALL(-20\%) O_3$ (1d)

254 Where “GLO” stands for the “global” source region.

255

256 The monthly-mean $R(O_3, *source\ region*, 20\%)$ values were averaged over the NAM
 257 region for the analysis and compared with the findings in the HTAP1 study (e.g., Fiore et al., 2009).
 258 It is worth mentioning that the rectangular source regions defined in HTAP1 were modified in
 259 HTAP2 to align with the geo-political borders. For EAS and SAS, the regions not overlapped by
 260 HTAP1 and HTAP2 are mostly in the less populated/polluted regions such as the northwestern
 261 China, according to the HTAP2 emission maps (http://edgar.jrc.ec.europa.eu/htap_v2/index.php).
 262 HTAP2’s EUR domain excludes certain regions in Russia/Belarussia/Ukraine, Middle East and
 263 North Africa that are included in HTAP1’s EUR domain. The impact of emissions over these
 264 regions on comparing the NAM $R(O_3, EUR, 20\%)$ values in HTAP1 and HTAP2 will be discussed
 265 in Section 3.2.1.

266

267 A unitless “Response to Extra-Regional Emission Reductions (RERER)” metric
 268 (Galmarini et al., 2017), as defined in eq. (2), was also calculated to measure the importance of
 269 local versus non-local sources to NAM’s O_3 levels:

270
$$RERER(O_3, NAM) = \frac{R(o3,non-NAM,20\%)}{R(o3,global,20\%)} = \frac{(NAMALL(-20\%) O_3 - GLOALL(-20\%) O_3)}{(BASE O_3 - GLOALL(-20\%) O_3)} \quad (2)$$

271 The denominator and numerator terms of RERER represent the impacts of global and non-NAM
 272 anthropogenic emissions on NAM O_3 , respectively. The higher the NAM RERER value is, the
 273 stronger impact from non-local sources on NAM is indicated. The RERER value can exceed 1,
 274 when emission reductions led to increasing concentrations (e.g. O_3 titration by nitrogen monoxide
 275 (NO)).

276

277 The STEM (version 2K3) regional simulations were then performed on a 60 km×60 km
 278 horizontal resolution (a typical coarse regional model resolution) grid over NAM within the
 279 domain defined in Figure 2a during May-June 2010. The meteorological conditions in spring 2010
 280 were compared with the climatology from the NCEP/NCAR reanalysis data for the 1981-2010
 281 period (Kalnay et al., 1996) in Huang et al. (2013b), concluding that this spring represents a period
 282 of stronger-than-climatological average spring trans-Pacific transport, based on a stronger
 283 meridional gradient in the North Pacific and higher Pacific/North American (PNA) indexes. This
 284 is consistent with the findings by Lin et al. (2014) that the El Niño conditions during the 09/10
 285 winter strengthened the trans-Pacific transport of Asian pollution in spring 2010. The mean near-
 286 surface air temperatures in the western US in this spring were lower than the climatology, with
 287 larger anomalies in the mountain states, which may have led to weaker local O_3 production and
 288 decomposition of the transported peroxyacyl nitrates (PAN). In contrast, higher-than-normal
 289 temperatures were found in the eastern US that favored anomalously strong local O_3 production.

290

291 STEM has been used to interpret the observations collected by satellites and during aircraft
 292 campaigns in the past decade (e.g., Carmichael et al., 2003a, b; Huang et al., 2010, 2013a, b, 2014,
 293 2015). STEM calculates gas-phase chemistry reactions based on the SAPRC 99 gaseous chemical
 294 mechanism (Carter, 2000) with thirty photolysis rates calculated online by the Tropospheric
 295 Ultraviolet-Visible radiation model (Madronich et al., 2002). Most of the key configurations of the

296 60 km base simulations are the same as those described in Lapina et al. (2014), i.e., meteorological
297 fields were pre-calculated by the Advanced Research Weather Research and Forecasting Model
298 (WRF-ARW, Skamarock et al., 2008) version 3.3.1 forced by the North American Regional
299 Reanalysis data (Mesinger et al., 2006), using a similar set of the physics configuration to those in
300 Huang et al. (2013a). Biomass burning emissions are from the Fire INventory from NCAR (FINN)
301 inventory version 1.0 (Wiedinmyer et al., 2011). Biogenic emissions were calculated by the Model
302 of Emissions of Gases and Aerosols from Nature (MEGAN) version 2.1 (Guenther et al., 2012),
303 driven by the WRF meteorology. Lightning NO_x emissions are generated following the method in
304 Allen et al. (2012), with the flash rates determined by the WRF convective precipitation and scaled
305 to the National Lightning Detection Network flash rates. A major difference of the STEM
306 simulations in this study from the Lapina (2014) study is that the anthropogenic emissions were
307 replaced with the monthly-mean HTAP2 inventory with no weekday-weekend variability applied,
308 rather than the earlier National Emission Inventory (NEI) 2005 in which the weekday-weekend
309 variability exists. This change can introduce uncertainty for some US regions where weekday-
310 weekend variability of some O₃ precursors' emissions was notable during the studied period (e.g.,
311 weekend NO_x emissions in southern California during spring/summer 2010 were 0.6-0.7 of the
312 weekday emissions as reported by Kim et al. (2016) and Brioude et al. (2013)), but this was done
313 to ensure consistency with the HTAP2 global model simulations, that also didn't use daily variable
314 emissions for any regions in the world. The VOC speciation for the SPRAC 99 chemical
315 mechanism in the NEI 2005 (ftp://aftp.fsl.noaa.gov/divisions/taq/emissions_data_2005) were
316 applied to break down the total NMVOC emissions provided in the HTAP2 inventory. The VOC
317 speciation based on the year of 2005 can be unrealistic for 2005 as well as 2010 as studies have
318 reported variable temporal changes of different VOC species in some US cities (e.g., Warneke et
319 al., 2012). The time-varying lateral and top boundary conditions in the STEM base simulations
320 were downscaled from three global models (i.e., 3 hourly SNU GEOS-Chem, 3 hourly ECMWF
321 C-IFS, and 6 hourly RAQMS) base simulations. In support of the SR relationship study to quantify
322 the East Asia anthropogenic impacts on the NAM, three STEM sensitivity simulations were also
323 conducted in which the STEM boundary conditions were downscaled from the EASALL(-20%)
324 sensitivity simulations by these three global models (Table 1b). All STEM simulated 3D chemical
325 fields were saved hourly for the convenience of calculating the US primary O₃ standard metric
326 MDA8 as well as the quantitative comparisons against the satellite Level 2 (L2) O₃ products. The
327 STEM base case surface O₃ performance and its O₃ sensitivities were also compared with those of
328 its boundary condition models as well as the multi- global model means. The latitude/longitude
329 ranges (20-50°N/130-65°W) of NAM for the global and regional model based sensitivity
330 calculations were selected to mainly account for the coverage of the STEM domain, which are
331 slightly different from the definition of North America in HTAP1.

332
333 Note that non-anthropogenic emission inputs used in STEM and its boundary condition
334 models differed, as summarized in Table 1c. Figure S1 shows detailed comparisons between
335 STEM and GEOS-Chem's non-anthropogenic (i.e., soil, lightning, biomass burning) NO_x
336 emission inputs, and their impacts on the modeled NAM background O₃ were included in Lapina
337 et al. (2014). Such quantitative comparisons will also be carried out between STEM and its other
338 boundary condition models in future studies.

339
340 2.2.2. Additional base and sensitivity simulations from selected models
341

342 In addition to the base and 20% EAS all-category emission perturbation simulations, the
343 global RAQMS model conducted a sensitivity simulation in which the East Asian anthropogenic
344 emissions were zeroed out, which was also used as STEM’s boundary conditions (Table 1b). We
345 calculate the “S<sub>O₃” metric (eq. (3)) using the O₃ sensitivities in STEM and RAQMS at the receptor
346 regions in response to both 20% and 100% of emission reductions, to explore the relationships
347 between the O₃ sensitivity and the size of the emission perturbation. A closer-to-one “S<sub>O₃” value
348 indicates higher scalability of the sensitivity based on the 20% emission perturbation method for
349 obtaining the full “contribution” of the East Asian anthropogenic emissions on the NAM O₃.</sub></sub>

350
351
$$S_{O_3} = R(O_3, \text{EAS}, 100\%) / R(O_3, \text{EAS}, 20\%) / 5 \quad (3)$$

352 Where: $R(O_3, \text{EAS}, 100\%) = \text{BASE } O_3 - \text{EASALL}(-100\%) O_3$
353

354 The RAQMS model also provided a base simulation that assimilated satellite O₃ products
355 from the Ozone Monitoring Instrument (OMI, Levelt et al., 2006) and Microwave Limb Sounder
356 (MLS, Livesey et al., 2008) (Pierce et al., 2007), which was used to help better understand the
357 regional model base run error sources, as well as for demonstrating the use of satellite observations
358 to help improve the representation of the trans-boundary pollution.
359

360 We also used a number of sensitivity simulations produced by the GEOS-Chem adjoint
361 model v35f in which the emissions from selected anthropogenic emission sectors (power&industry,
362 transportation, residential) or individual O₃ precursor chemical species (NO_x, VOC, CO) over the
363 East Asia were reduced by 20%. Additional simulations for the 2008-2009 periods by the SNU
364 GEOS-Chem were also utilized to quantify the East Asia and non-NAM anthropogenic source
365 impacts in comparison with the 2010 conditions that we mainly focus on in this study.
366

367 2.3. *In-situ and satellite observations*

368 2.3.1. In-situ observations

369 Over the receptor NAM, the hourly O₃ observations at the Clean Air Status and Trends
370 Network (CASTNET, <http://epa.gov/castnet/javaweb/index.html>) sites were used to evaluate the
371 global and regional models’ base simulations in four subregions: western US (i.e., the EPA regions
372 8, 9, 10); southern US (i.e., the EPA regions 4 and 6), the Midwest (i.e., the EPA regions 5 and 7),
373 and the northeast (i.e., the EPA regions 1-3). The numbers of sites used in global and regional
374 models’ evaluation in each US subregion are summarized in Tables 2-3. The locations of these
375 sites and the subregions they belong to are indicated in Figure 2a, overlaid on a model-based terrain
376 height map. A majority of the CASTNET sites in the western US are located at high elevation (>1
377 km) remote or rural regions, more susceptible to the trans-boundary pollution (e.g., Jaffe, 2011).
378 Most of the sites in the other three subregions are located in low elevation regions, mainly affected
379 by local and regional pollution. The model-based terrain heights fairly well represent the reality
380 on subregional scale – the differences between the actual and model-based subregional mean
381 terrain heights at the CASTNET sites are smaller than 0.1 km (Table 3).
382

383 During May-June 2010, intense ozonesonde measurements were made at multiple
384 California locations (Cooper et al., 2011), in support of the NOAA “California Nexus (CalNex):
385 Research at the Nexus of Air Quality and Climate Change” field experiment (Ryerson et al., 2013).
386 They have been used to evaluate the simulated O₃ vertical profiles by the HTAP2 participating

387 models. The detailed evaluation results have been shown by Cooper et al. (2016), and will be
388 covered by subsequent publications.

389
390 Over HTAP2's EAS source region, the global models' O₃ performance was evaluated
391 against the monthly-mean surface in-situ O₃ measurements at 11 sites within the Acid Deposition
392 Monitoring Network in East Asia (EANET, <http://www.eanet.asia>) that had data throughout the
393 year of 2010. These include eight Japanese and three Korean sites (Figure 3a), all of which are
394 located at low elevation regions (2-150 m). The reported monthly mean observations at these sites
395 were based on weekly or daily sampled data, varying among sites.

396 397 2.3.2. Satellite products

398
399 In two case studies of high O₃ episodes, L2 and L3 O₃ and CO retrievals from several
400 satellite instruments were used to assess the impacts of trans-Pacific pollution transport and
401 stratospheric O₃ intrusions on NAM O₃ levels in early May. These include: 1) the early afternoon
402 O₃ and CO profiles version 5 from the Tropospheric Emission Spectrometer (TES) (Beer et al.,
403 2001; Beer, 2006) on the Aura satellite; 2) the mid-morning O₃ profiles from the METOP-Infrared
404 Atmospheric Sounding Interferometer (IASI), which were retrieved using the Jet Propulsion
405 Laboratory (JPL) TES optimal estimation retrieval algorithm (Bowman et al., 2006) for selected
406 areas including the western US (Oetjen et al., 2014, 2016); as well as 3) the early afternoon L3 O₃
407 and CO maps (version 6, 1°×1°) from the Aqua Atmospheric Infrared Sounder (AIRS) instrument.
408 The TES tropospheric O₃ retrieval is often sensitive to the mid- to lower free troposphere, and O₃
409 at these altitudes in the Eastern Pacific is known to possibly impact the downwind US surface air
410 quality at later times (Huang et al., 2010; Parrish et al., 2010). TES O₃ is generally positively
411 biased by <15% relative to high accuracy/precision reference datasets (e.g., Verstraeten et al.,
412 2013). Although IASI is in general less sensitive than TES due to its coarse spectral resolution, the
413 681–316 hPa partial column-averaged O₃ mixing ratios in the JPL product agree well with TES
414 O₃ for the 2008–2011 period with a -3.9 ppbv offset (Oetjen et al., 2016). Note that IASI O₃ data
415 are processed operationally in Europe using a different algorithm. For this work we used O₃
416 profiles from TES and IASI processed using a consistent algorithm at JPL, although the latter set
417 of data represents only a small subset of the full set of the IASI radiance measurements. The IASI
418 and TES L2 O₃ profiles (screened by the retrieval quality and the C-Curve flags) were used to
419 evaluate the STEM O₃ vertical distributions in the different base simulations, and the satellite
420 observation operators were applied in these comparisons. Taking TES as an example, its
421 observation operator h_z for O₃ is written in (4):

$$422 \quad h_z = z_c + A_{\text{TES}} (\ln(F_{\text{TES}}(c)) - z_c) \quad (4)$$

423 where z_c is the natural log form of the TES constraint vector (a priori) in volume mixing ratio.
424 A_{TES} is the averaging kernel matrix reflecting the sensitivity of retrieval to changes in the true state
425 (Rodgers, 2000). F_{TES} projects the modeled O₃ concentration fields c to the TES grid using spatial
426 and temporal interpolation. The exponential of h_z is then used to compute the mismatches between
427 the model and TES O₃ retrievals as the model evaluation. A small mismatch between model with
428 the satellite observation operators and the satellite retrievals may indicate either good model
429 performance or may be the low sensitivity of the retrievals to the true O₃ profile. AIRS O₃ is
430 sensitive to the altitudes near the tropopause, with positive biases over the ozonesondes in the
431 upper troposphere (e.g., Bian et al., 2007); AIRS CO is most sensitive to 300–600 hPa (Warner et
432 al., 2007) and is frequently used together with the AIRS O₃ to distinguish the stratospheric O₃

433 intrusions from long-range transported anthropogenic or biomass burning pollution. We use the
434 L3 AIRS products in this study to get a broad overview of the areas that are strongly impacted by
435 the stratospheric O₃ intrusions or/and LRT of pollution.

436
437 The bottom-up NO_x emissions from the HTAP2 inventory were assessed on a monthly base
438 by comparing the GEOS-Chem nitrogen dioxide (NO₂) columns with the de-striped KNMI (Royal
439 Netherlands Meteorological Institute) OMI column NO₂ product version 2.0 (Boersma et al.,
440 2011a, b). For this model evaluation against the OMI L2 products, the NO₂ fields calculated by the
441 GEOS-Chem adjoint model were saved daily at 13:30 local solar time, roughly coinciding with
442 the Aura and Aqua overpassing times. Other parameters used in the model column calculations
443 came from the GEOS-5/GEOS-Chem monthly mean conditions. The OMI data that passed the
444 tropospheric quality flag at 13-14 local time were selected based on the following screening criteria:
445 surface albedo<0.3; cloud fraction<0.2; solar zenith angle <75°; and viewing zenith angle <45°.
446 The averaging kernels (Eskes and Boersma, 2003) and Air Mass Factors (AMFs) in the KNMI
447 product were used to calculate the modeled tropospheric NO₂ vertical columns comparable to the
448 OMI's. Details of the method to compare the model-based NO₂ columns with the KNMI OMI's
449 can be found in Huang et al. (2014).

450

451 **3. Results and Discussions**

452 *3.1. Evaluation of the HTAP2 bottom-up NO_x emissions and the model base simulations*

453 3.1.1. Evaluation of the bottom-up NO_x emissions

454

455 The comparison of the GEOS-Chem adjoint NO₂ columns with the OMI product was used
456 to help assess the bottom-up HTAP2 NO_x emissions. Figure 4 shows that NO₂ columns from
457 GEOS-Chem's base simulations over the US are overall overestimated. While grid-scale
458 differences in NO₂ columns may not be directly indicative of emissions biases (Qu et al., 2016),
459 these discrepancies are possibly due to a positive bias in the bottom-up emissions, mainly from the
460 anthropogenic sources, which have also been pointed out by Anderson et al. (2014) and Travis et
461 al. (2016). Larger OMI-model disagreement was found over the central/eastern US in June 2010
462 than in May, likely also due to the uncertainty in GEOS-Chem's soil or lightning NO_x emissions,
463 which appear to be high over these regions (Figure S1). The NO₂ columns in the GEOS-Chem
464 base simulation were overestimated in many northern China rural areas and underpredicted in a
465 few urban areas in the East Asia as well as a broad area in the southwestern China. The mismatches
466 between model and OMI NO₂ fell within the ranges of the comparison between the GOME2 NO₂
467 column product and six models' simulations over China in summer 2008 (Quennehen et al., 2016).
468 Also, the use of monthly-mean anthropogenic emissions as well as the overall rough treatment of
469 emission height and temporal profiles can be sources of uncertainty. These global model
470 evaluation results suggest that the EAS-NAM SR relationships analyzed using this inventory may
471 overall overestimate the NAM local contribution and underestimate the EAS contribution—Under
472 different chemical regimes, this statement would also rely on the quality of other O₃ precursors'
473 emissions in the HTAP2 inventory, and they may be associated with variable uncertainties
474 depending on the species or emission sector as introduced in Section 2.1. Therefore, careful
475 assessment of other key O₃ precursors' emissions in the inventory is needed in the future work. It
476 is important to note that uncertainty in satellite retrievals can prevent us from producing accurate
477 assessment on emissions (e.g., van Noije et al., 2006), and this comparison does not account for
478 the biases in the used OMI data, and would be further validated by using other OMI NO₂ products

479 as well as the bias-corrected (if applicable) in-situ NO₂ measurements. We also recommend more
480 global models to save their calculations more frequently, at least near the satellite overpassing
481 times, for a more comprehensive assessment of the emission inventory and a better understanding
482 of the model biases.

483 484 3.1.2. Evaluation of the global model O₃ performance in NAM and EAS

485
486 The monthly-mean surface O₃ from multiple global models' free runs was evaluated with
487 the CASTNET observations, at the stations with 95% of the hourly O₃ observation completeness
488 for the 1 May-30 June 2010 period. The mean biases and RMSEs for these two months were
489 summarized in Table 2a by US subregions. The three boundary condition-model as well as the
490 eight-model ensembles overall underpredicted O₃ in the western US (by ~3-6 ppbv), similar to the
491 HTAP1 model performance over these regions for May-June 2001 presented in Fiore et al. (2009).
492 This can be due to the underestimated trans-boundary pollution (as indicated by the evaluation of
493 modeled O₃ profiles with ozonesondes and satellite O₃ products). In addition, the coarser model
494 resolutions are less capable of resolving the local features that influence the pollutants' import
495 processes, chemical transformation, as well as regional processes such as the cross-state pollution
496 transport over complex terrains. The global RAQMS base simulation with satellite assimilation
497 improved the free tropospheric O₃ structure as its comparisons with the ozonesondes shows, which
498 also enhanced the simulated monthly-mean surface O₃ by up to >10 ppbv in the western US and
499 some coastal areas in the southeastern US (Figure S2, left). The global models overall significantly
500 overestimated O₃ in the other three subregions (by 8-12 ppbv), close to HTAP1 model performance
501 for May-June 2001 over the similar areas (Fiore et al., 2009) and in the Lapina et al. (2014) study
502 for 2010, in large part due to the uncertainties in the bottom-up emissions as discussed in Section
503 3.1.1. Satellite assimilation led to 2-6 ppbv higher RAQMS surface O₃ in the
504 central/southern/eastern US than in its free simulation, which are associated with higher positive
505 biases.

506
507 The surface O₃ performance by individual global models varies significantly, e.g., with the
508 RMSEs at all CASTNET sites ranging from ~9 ppbv to >15 ppbv (Table 2b). As reported in the
509 literature (e.g., Geddes et al., 2016; Travis et al., 2016), the representation of land use/land cover,
510 boundary layer mixing and chemistry can be sources of uncertainty for certain global model (i.e.,
511 GEOS-Chem), but how serious these issues were in the other models need to be investigated
512 further. Some other possible reasons include the variation of these models' non-anthropogenic
513 emission inputs and chemical mechanisms (Table 1c). Future work should emphasize on
514 evaluating and comparing all models on process level to better understand their performance.
515 Except in the northeastern US, the eight-model ensembles show better agreement with the
516 CASTNET O₃ observations than the three boundary condition-model ensemble. Overall the three-
517 model ensemble only outperforms one model but the eight-model ensemble outperforms seven
518 individuals. This reflects that averaging the results from a larger number of models in this case
519 more effectively cancelled out the positive or negative biases from the individual models.

520
521 The monthly-mean surface O₃ from multiple global models' free runs was also evaluated
522 with the EANET observations. Among the three boundary condition models, GEOS-Chem
523 produced higher O₃ than the other two throughout the year, and C-IFS O₃ is the lowest from April
524 to December. The three-model and eight-model ensembles are lower than the surface O₃

525 observations by <10 ppbv during high O₃ seasons (winter/spring), but show substantial (>10 ppbv)
526 positive biases during low O₃ seasons especially in July and August (Figure 3b), similar to the
527 HTAP1 model performance over Japan in 2001 (Fiore et al., 2009). During May-June 2010,
528 generally the models performed better at the Japanese sites than at the Korean sites (Table 2c),
529 with significant positive biases occurring at low O₃ regions (e.g., in central Japan) and negative
530 biases found at high O₃ regions, mainly owing to the uncertainty in the local and upwind emissions.
531 The different approaches to generate the monthly-mean modeled and the observed O₃ data may
532 have also contributed to these model-observation discrepancies. Overall O₃ performance by
533 individual models varies less significantly than at the CASTNET sites, with RMSEs ranging from
534 8.6 ppbv to ~13 ppbv (Table 2b). The three-model ensemble outperforms two individual models,
535 and the eight-model ensemble outperforms six individual models. Unlike at the CASTNET sites,
536 the three-model ensemble agrees better with the observations than the eight-model ensemble
537 (Table 2c).

538

539 3.1.3. Evaluation of the STEM regional base simulations w/ three sets of boundary conditions

540

541 The three STEM base simulations using different boundary conditions were evaluated with
542 the hourly O₃ observations at the CASTNET sites in the four US subregions. The evaluation
543 included the 8 May-30 June 2010 period to exclude the results during the one-week spin-up period.
544 The time series plots of observed and modeled O₃ at the western US CASTNET sites show that
545 STEM was capable of capturing several high O₃ periods, and it produced larger biases during the
546 nighttime (Figure 2c), as a result of the poorer WRF performance. Figure 2c and the evaluation
547 statistics in Table 3a-b indicate that STEM/C-IFS O₃ concentrations are associated with the highest
548 positive bias and RMSE, while the STEM/GEOS-Chem and STEM/RAQMS predictions were
549 positively and negatively biased by less than 2 ppbv, respectively, with similar RMSEs and
550 correlations with the observations. The quality of the three STEM simulation mean is closest to
551 the STEM/GEOS-Chem run, with the mean bias/RMSE of ~1.6/4.9 ppbv, much better than the
552 three-boundary model ensemble (-5.7/10.4 ppbv). However, this good performance can be a net
553 effect of incorrect partitioning between the trans-boundary and local source contributions, with the
554 former being underestimated and offsetting the overestimation of the latter. Switching the STEM
555 chemical boundary conditions to the assimilated RAQMS base simulation led to increases in the
556 simulated surface O₃ concentrations by >9 ppbv in the western US (Figure S2, right), associated
557 with higher positive biases (due to several factors discussed in the next paragraph). Regional-scale
558 assimilation could further reduce uncertainties introduced from regional meteorological and
559 emission inputs to obtain better modeled total O₃ and the partitioning of trans-boundary versus US
560 contributions (e.g., Huang et al., 2015).

561

562 The three STEM base simulations all significantly overpredicted O₃ over the rest of the US
563 in part due to the uncertainties in NO_x emissions, with the STEM/RAQMS associated with the
564 lowest RMSEs and mean biases, but STEM/C-IFS correlated best with the observations (Table
565 3b). These positive biases are higher than the global model ensembles', which can partially result
566 from the possible unrealistic VOC speciation of the emission inventory and the SAPRC 99
567 chemical mechanism: Although SAPRC mechanisms have been used in air quality modeling for
568 regulatory applications in some US states such as California, they usually produced higher O₃ than
569 other mechanisms such as the CB04 and the CB05 (which were used by some HTAP2 global
570 models, see Table 1c) over the US, and the comparisons between SAPRC 99 and SAPRC 2007

571 are still in progress (e.g., Luecken et al., 2008; Zhang et al., 2012; Cai et al., 2011). It is important
572 to timely update the chemical mechanisms in the chemistry models, and we also suggest to timely
573 upgrade the VOC speciation in the bottom-up emission inventories in the US to benefit the air
574 quality modeling. Additionally, the uncertainty from non-anthropogenic emissions, such as the
575 biogenic VOC emissions from WRF/MEGAN which is known to often have positive biases, can
576 be another cause: As Hogrefe et al. (2011) presented, the MEGAN emissions resulted in a higher
577 O₃ response to hypothetical anthropogenic NO_x emission reductions compared with another set of
578 biogenic emission input. Huang et al. (2017) showed that MEGAN's positive biases are in part
579 due to the positively-biased temperature and radiation in WRF, and reducing ~2°C in WRF's
580 temperature biases using a different land initialization approach led to ~20% decreases in
581 MEGAN's isoprene emission estimates in September 2013 over some southeastern US regions.
582 These temperature and radiation biases, can also be important sources of uncertainty in the
583 modeled O₃ production. Quantifying the impacts of overestimated biogenic emissions and the
584 biased weather fields that contributed to the biases in emissions on the modeled O₃ is still an
585 ongoing work. Some existing studies also reported O₃ and NO₂ biases from other regional models
586 in the eastern US, due to the chemical mechanism and biases in NO_x and biogenic VOC emissions
587 (e.g., Canty et al., 2015). We anticipate that the results from the Air Quality Model Evaluation
588 International Initiative (AQMEII) experiment (e.g., Schere et al., 2012; Solazzo et al., 2012;
589 Galmarini et al., 2015, 2017), which involves more regional model simulations over the US with
590 the similar set of boundary conditions but different chemical mechanisms and non-anthropogenic
591 emission inputs, can help better understand the causes of errors in the simulated total O₃.

592

593 3.2. *The NAM surface O₃ sensitivity to extra-regional anthropogenic pollutants*

594 3.2.1. Global model ensembles

595

596 The impact of all foreign (i.e. non-NAM) anthropogenic sources on NAM surface O₃ was
597 first explored, including the spatial distributions of the RERER metric (eq. (2)) based on various
598 global models' simulations (Figure 5), and the domain wide mean sensitivities R (O₃, non-NAM,
599 20%) (eq. (1d)) (Figure 6). Across the NAM, the strongest impacts were found in spring time
600 (March-April-May, larger than 1.5 ppbv in average over the domain) and the weakest impacts are
601 shown during the summertime (June-July-August, 1.0-1.3 ppbv), consistent with the existing
602 knowledge on the seasonal variability of the non-local pollution impacts on NAM for other years
603 (e.g., Fiore et al., 2009; Reidmiller et al., 2009). All global models indicate strong non-NAM
604 anthropogenic source impacts on the western US mainly due to the impact of its high elevation,
605 and also near the US-Mexico border areas, especially southern Texas, due to their vicinity to the
606 Mexican (not included in the NAM source regions, see Figure 1) emission sources. Over the
607 western states, stronger non-local impacts were reflected from the results based on higher-
608 horizontal resolution global models (e.g., the >0.6 RERER values from the half degree EMEP
609 model, corresponding to its higher R(O₃, non-NAM, 20%) values than the other models'), similar
610 to the findings in previous modeling studies (Lin et al., 2010, 2012a). Although on a coarse
611 horizontal resolution of 2.8°, OsloCTM3 suggests stronger extra-regional source influences on the
612 northwestern US and the US-Canada border regions than the other models. Its largest number of
613 vertical layers among all global models might be a cause. Larger-than-1 RERER values are often
614 seen near the urban areas and large point sources due to the titration, especially evident from the
615 higher resolution model results. The R(O₃, EAS, 20%) values are larger than 1/3 of the R(O₃, non-
616 NAM, 20%) (0.2-0.5 ppbv from April to June), more than 3-4 times higher than R(O₃, EUR, 20%)

617 and $R(\text{O}_3, \text{SAS}, 20\%)$. Note that all eight models contributed to the $R(\text{O}_3, \text{EAS}, 20\%)$ calculations,
618 but one or two models did not provide all necessary sensitivity runs to compute the RERER, $R(\text{O}_3,$
619 $\text{non-NAM}, 20\%)$, $R(\text{O}_3, \text{EUR}, 20\%)$, or $R(\text{O}_3, \text{SAS}, 20\%)$.

620
621 Comparing to the HTAP1 modeling results, the magnitudes of $R(\text{O}_3, \text{EUR}, 20\%)$ from this
622 study are smaller by a factor of 2-3; In contrast, the $R(\text{O}_3, \text{non-NAM}, 20\%)$ and $R(\text{O}_3, \text{EAS}, 20\%)$
623 values are >50% higher than the HTAP1 modeling results. The different HTAP1 and HTAP2
624 results are possibly due to the following three reasons: 1) the substantial improvement in the
625 European air quality over the past decades that is shown in Crippa et al. (2016) and Pouliot et al.
626 (2015), which contrasts with the growing anthropogenic emissions from the East Asia and other
627 developing countries during 2001-2010; 2) the changes in the HTAP2 experiment setup from
628 HTAP1. This includes the differences in the participating models, and the different region
629 definitions, e.g., EUR by HTAP1's definition includes regions in Russia/Belarus/Ukraine,
630 Middle East and North Africa that are excluded from the HTAP2's EUR domain. For EAS and
631 SAS, however, the regions not overlapped by HTAP1 and HTAP2 are mostly in the less
632 populated/polluted regions; 3) the stronger trans-Pacific transport in 2010 than in 2000-2001, as
633 first introduced in Section 2.2.1. Interannual variability of $R(\text{O}_3, \text{EAS}, 20\%)$ and $R(\text{O}_3, \text{non-NAM},$
634 $20\%)$ is also found between 2010 and 2008-2009, based on the SNU GEOS-Chem calculations
635 (Figure S3). Foreign anthropogenic pollution impact on NAM was stronger in 2010 than in 2008-
636 2009, especially in April-May. This can be in part due to the higher O_3 precursors' emissions in
637 2010 from extra-regions including the East Asia (Table S1), as well as the spring 2010
638 meteorological conditions that favored the trans-Pacific pollution transport.

639
640 These monthly- and regional-mean $R(\text{O}_3, \text{EAS}, 20\%)$ values suggest that despite dilution
641 along the great transport distance, the EAS anthropogenic sources still had distinguishable impact
642 on the NAM surface O_3 . Similar to the findings from the HTAP1 studies, the large intermodel
643 variability (as indicated in Table 4) in the estimates of intercontinental SR relationships indicates
644 the uncertainties of these models in representing the key atmospheric processes which needs more
645 investigations in the future. Figure 6b compares the $R(\text{O}_3, \text{EAS}, 20\%)$ estimated by individual
646 boundary condition models, their ensemble mean sensitivities, and the eight-global model mean.
647 The averaged $R(\text{O}_3, \text{EAS}, 20\%)$ from the boundary condition model results are smaller than the
648 eight-global model mean, and except for July-October 2010, GEOS-Chem gives higher $R(\text{O}_3, \text{EAS},$
649 $20\%)$ than RAQMS and C-IFS, consistent with its highest O_3 prediction in the EAS source region
650 (Figure 3b). Overall, $R(\text{O}_3, \text{EAS}, 20\%)$ and its intermodel differences are much smaller than the
651 biases of the modeled total O_3 in NAM. Other factors can contribute more significantly to the
652 biases in the modeled total O_3 , such as the stratospheric O_3 intrusion and the local O_3 formation,
653 and assessing the impacts from these factors would be also helpful for understanding the
654 uncertainties in the modeled O_3 .

655
656 The O_3 sensitivities in response to the perturbations of individual species or sector
657 emissions in East Asia, estimated by the GEOS-Chem adjoint model, were also analyzed (Figure
658 S3). These sensitivities show similar seasonal variability to $R(\text{O}_3, \text{EAS}, 20\%)$, with the values
659 ~twice as high in the spring than in summer, also consistent with the results on previous years
660 based on the 20% emission perturbation approach (e.g., Fiore et al., 2009; Brown-Steiner and Hess,
661 2011; Emmons et al., 2012). However, this seasonal variability is weaker than the results based on
662 the tagged tracer approach for earlier years: Using the CAM-Chem model, Brown-Steiner and

663 Hess (2011) reported that during the springtime, Asian O₃ created from the anthropogenic/biofuel
664 NO_x emissions affected NAM O₃ ~three times as strongly as in summer. This is because the
665 nonlinear O₃ chemistry, which is stronger outside of summer, caused larger O₃ responses to a 100%
666 reduction of NO_x emissions than 5 times of the O₃ responses to a 20% reduction of NO_x emissions.
667 The EAS anthropogenic NO_x emissions more strongly impacted the NAM surface O₃ than the
668 other major O₃ precursors, similar to the findings in Fiore et al. (2009) and Reidmiller et al. (2009)
669 using the perturbation approach, as well as the conclusions in Lapina et al. (2014) based on the
670 adjoint sensitivity analyses. Emissions from the power&industrial sectors are higher in East Asia
671 than the other sectors (Table S1), resulting in its stronger influences on the NAM surface O₃. As
672 the observed NO₂ columns started to drop since 2010 due to the effective denitration devices
673 implemented at the Chinese power and industrial plants (e.g., Liu et al., 2016), depending on the
674 changes in the VOC emissions, it is anticipated to see different R(O₃, EAS, 20%) values for the
675 years after 2010. Therefore, continued studies to assess the East Asian anthropogenic pollution
676 impacts on NAM during more recent years is needed. As emissions from various source sectors
677 can differ by their emitted altitudes and temporal (from diurnal to seasonal) profiles, efforts should
678 also be placed to have the models timely update the heights and temporal profiles of the emissions
679 from those various sectors.

680

681 3.2.2. Regional model sensitivities and their connections with the boundary condition models'

682

683 The monthly-mean STEM surface R(O₃, EAS, 20%) sensitivities based on different
684 boundary condition models were inter-compared, and also compared with the R(O₃, EAS, 20%)
685 estimated by their boundary condition models as well as the global model ensemble mean (Figure
686 7). For both May and June 2010, the domain-wide mean R(O₃, EAS, 20%) values from
687 STEM/RAQMS were higher than the estimates from RAQMS by 0.03 ppbv; the STEM/GEOS-
688 Chem R(O₃, EAS, 20%) values are lower than those of GEOS-Chem by 0.01-0.06 ppbv, and the
689 STEM/C-IFS R(O₃, EAS, 20%) is 0.02 ppbv higher than C-IFS's in June but slightly (<<0.01 ppbv)
690 lower in May. These differences are overall smaller than the inter-global model differences, and
691 can be due to various factors including the uncertainties in boundary condition chemical species
692 mapping, and the different meteorological/terrain fields/chemistry in the global and regional model
693 pairs. The STEM R(O₃, EAS, 20%) ensemble mean values, however, are less than 0.02 ppbv
694 different from its boundary condition model's ensemble mean for both months. The STEM R(O₃,
695 EAS, 20%) ensemble mean value in June is also close to the eight-global model ensemble mean,
696 but is ~0.05 ppbv lower than the eight-model mean in May. Choosing other/more global model
697 outputs as STEM's boundary conditions may lead to different STEM ensemble mean R(O₃, EAS,
698 20%) estimates. We also found that the period mean R(O₃, EAS, 20%) of ~0.2 ppbv sampled only
699 at the CASTNET sites (Table 3a) are smaller than those averaged in all model grids. This indicates
700 that currently the sparsely distributed surface network (especially over the western US that is more
701 strongly affected by the extra-regional sources than the other US regions) may miss many LRT
702 episodes that impact the NAM. The planned geostationary satellites with ~2-5 km footprint sizes
703 and hourly sampling frequency (Hilsenrath and Chance, 2013; Zoogman et al., 2017) will help
704 better capture the high O₃ and LRT episodes in these regions.

705

706 The spatial patterns of the monthly-mean STEM surface R(O₃, EAS, 20%) sensitivities
707 based on the three boundary condition models are notably different, but overall resemble what's
708 estimated by the corresponding boundary condition model, and the STEM sensitivities show more

709 local details in certain high elevation regions in the US west (Figure 8 shows the June 2010
710 conditions as an example). These different sensitivities were investigated further, by examining
711 the $R(O_3, \text{EAS}, 20\%)$ values near the source regions (i.e., East Asia) as well as near the receptor
712 regions (Figure 9). More East Asian anthropogenic O_3 seems to be transported at the upper
713 troposphere in RAQMS than in the other two models. GEOS-Chem and RAQMS $R(O_3, \text{EAS}, 20\%)$
714 sensitivities are similar over the EAS as well as the 500-900 hPa near the receptor in the eastern
715 Pacific (at $\sim 135^\circ\text{W}$), the altitudes US surface O_3 are most strongly sensitive to during the
716 summertime as concluded from previous studies (e.g., Huang et al., 2010, 2013a; Parrish et al.,
717 2010). Despite the close NAM domain-wide mean values from the STEM/GEOS-Chem and
718 STEM/RAQMS, the spatial patterns of $R(O_3, \text{EAS}, 20\%)$ over NAM differ in these two cases,
719 with the latter case showing sharper gradients especially in the western US, partially due to the
720 impact of its higher horizontal resolution. The $R(O_3, \text{EAS}, 20\%)$ values from STEM/C-IFS are
721 lower than from the other two cases both near the sources and at (near) NAM. The STEM surface
722 (also near surface, not shown in figures) $R(O_3, \text{EAS}, 20\%)$ does not spatially correlate well with
723 the column $R(O_3, \text{EAS}, 20\%)$, the latter of which contributed more to the base case O_3 columns,
724 indicating that a good portion of the transported East Asian pollution did not descend to the lower
725 altitudes to impact the boundary layer/ground level air quality. An additional regional simulation
726 was performed in which the STEM boundary conditions were downscaled from a RAQMS
727 simulation without the East Asian anthropogenic emissions. The non-linear emission perturbation-
728 O_3 response relationships, as the larger-than-1 S_{O_3} metric (eq. (3)) indicate, are seen across the
729 domain, for both the surface and column O_3 (Figure 8). S_{O_3} for column O_3 , ranging from 1.15-1.25
730 in most regions, are overall ~ 0.05 higher than S_{O_3} for the surface O_3 . Therefore, the full source
731 contribution obtained by linearly scaling the receptor regional mean O_3 sensitivity to the 20%
732 reduction in the source region emissions may be underestimated by at least $\sim 10\%$.

733

734 3.2.3. Regional model MDA8 sensitivities on all days and during the O_3 exceedances

735 The temporal variability of the STEM $R(O_3, \text{EAS}, 20\%)$ ensemble sensitivities were also
736 studied. For most US subregions, 3-6 LRT episodes (defined as when the sensitivities are above
737 the period mean) were identified during May-June. Only in certain regions, we find that the
738 planetary boundary layer heights (PBLHs) were higher during the LRT episodes (i.e., the daily
739 daytime-mean $R(O_3, \text{EAS}, 20\%)$ and PBLHs show medium/strong positive correlations ($r > 0.5$)),
740 as these correlations may have been complicated by the relationships between the PBLHs and the
741 local influences. Throughout this period, the hourly $R(O_3, \text{EAS}, 20\%)$ and the observed O_3 at the
742 surface CASTNET sites are weakly correlated (Table 3a), but they display similar diurnal cycles
743 (e.g., Figures 2c and 2d for the western US sites), possibly because the deeper boundary layer
744 depth during the daytime enhanced entrainment down-mixing of the extra-regional pollutants to
745 the surface. The identified diurnal variability of the $R(O_3, \text{EAS}, 20\%)$ can cause differences in the
746 calculated MDA8 and all-hour mean $R(O_3, \text{EAS}, 20\%)$ values. Figure S4 shows that the mean
747 $R(\text{MDA8}, \text{EAS}, 20\%)$ values, usually at daytimes, are higher than the all-hour averaged $R(O_3,$
748 $\text{EAS}, 20\%)$ in most STEM model grids during both months. Therefore, it is important for more
749 HTAP2 participating models to save their outputs hourly in order to conveniently compute the
750 policy-relevant metrics for the O_3 sensitivities. Also, the hourly sampling frequency of the planned
751 geostationary satellites is anticipated to be more helpful for evaluating the impacts of the LRT
752 episodes.

753

754 The STEM R(MDA8, EAS, 20%) in all model grids within the four US subregions were
755 averaged on all days during May-June 2010 and only on the days when the simulated total MDA8
756 O₃ is over 70 ppbv (Figure 10). These sensitivities also show appreciable spatial variability: from
757 0.35-0.58 ppbv in the western US (also with the largest standard deviations, not shown), which is
758 slightly higher than the HTAP1 results reported by Reidmiller et al. (2009) for Spring 2001, to
759 ~0.1-0.25 ppbv in the rest three subregions, which is close to the Reidmiller et al. (2009) results.
760

761 Comparing the solid bar plots in Figures 10-11, we found that on all days in the three non-
762 western subregions, R(MDA8, EAS, 20%) values sampled at CASTNET sites are slightly smaller
763 than those computed for all model grids, while in the non-western states the opposite differences
764 are seen. This again suggests that expanding observation network would help better capture the
765 high O₃ and LRT episodes.
766

767 Figure 10 suggests smaller R(MDA8, EAS, 20%) values during the high O₃ days in all
768 subregions. However, STEM's total O₃ concentrations at CASTNET sites during the O₃
769 exceedances were substantially overpredicted in non-western US regions while significantly
770 underpredicted in the western US (see mean biases above the bar plots in Figure 11). Therefore,
771 the R(MDA8, EAS, 20%) values shown in Figure 10 during the model-based periods of O₃
772 exceedances can represent the sensitivities during the actual periods of O₃ compliance in non-
773 western US regions, and may not represent the sensitivities during all actual O₃ exceedances in the
774 western US. Figures 11-12 show that if calculated only at the CASTNET sites during the
775 exceedances, in non-western US regions, R(MDA8, EAS, 20%) is 0.02-0.07 ppbv smaller during
776 the high O₃ total days. This is qualitatively consistent with the findings in Reidmiller et al. (2009),
777 and is possibly because that the LRT impacts were stronger on some days with good dispersion
778 conditions when the NAAQS was not exceeded, but weaker on some high O₃ days under stagnant
779 conditions. In contrast, western US R(MDA8, EAS, 20%) at CASTNET sites was ~0.05 ppbv
780 higher on high O₃ days than for all days, and this differences are larger in rural/remote areas where
781 local influences are less dominant. As a result, the medium/strong positive correlations are found
782 between modeled LRT of pollution and the total O₃ in these regions (Table 3a; Lin et al., 2012a).
783

784 3.3. Case studies of spring (9 May) and summer (10 June) LRT events mixed with stratospheric 785 O₃ intrusions 786

787 Lin et al. (2012a, b) and Neuman et al. (2012) showed that the trans-Pacific pollution
788 transport intensely impacted the western US during 8-10 May, 2010, intermingled with a
789 stratospheric intrusion that contributed to at least 1/3 of the total O₃ in some high elevation regions.
790 This episode is indeed indicated by the O₃ and CO products from AIRS and TES at ~500 hPa over
791 the Eastern Pacific (Figure 13), and the observed TES and IASI O₃ profiles over the western US
792 indicated elevated O₃ levels (>80 ppbv) at 700-900 hPa. Huang et al. (2013b) found that the
793 meteorological conditions during this period (i.e., a strong jet at ~700 hPa with wind speed >20
794 m/s shifted southwesterly when passing the southern California and continued to travel towards
795 the mountain states), along with the orographic lifting, efficiently exported the southern California
796 anthropogenic pollution, which was chemically coupled with the extra-regional pollution and
797 significantly enhanced the O₃ levels in the US intermountain west.
798

799 We selected this episode to compare the STEM surface total O₃ concentrations as well as
800 the R(O₃, EAS, 20%) sensitivities based on the different HTAP2 boundary condition models.
801 Figure 14 evaluates the simulated O₃ profiles in the western US from several STEM base
802 simulations against the TES and IASI O₃ retrievals, and Figures 15a-d indicate the performance of
803 the daily surface total MDA8 O₃ from these simulations. We found that the underestimated free
804 tropospheric O₃ from the STEM simulations that used any single free-running chemical boundary
805 conditions contributed to the underestimated STEM surface O₃ in the high elevation mountain
806 states: e.g., by 9-14 ppbv at three CASTNET sites (Grand Canyon National Park (NP), AZ;
807 Canyonlands NP, UT; and Rocky Mountain NP, CO) where O₃ exceedances were observed. The
808 unsatisfactory performance by free-running global models during high O₃ events would pose
809 difficulties for regional models (regardless of their resolutions and other configurations,
810 parameterization) to accurately estimate the SR relationships using boundary conditions
811 downscaled from these model runs. The STEM base simulation using the RAQMS assimilated
812 fields as the boundary conditions, agrees most with the observed O₃ at the CASTNET sites, as well
813 as the TES and IASI O₃ profiles in the western states. Similar to the conclusions drawn in Huang
814 et al. (2010, 2015) for summer 2008, we again demonstrated the robustness of satellite chemical
815 data assimilation for improving the boundary condition models' O₃ performance. As the
816 enhancement of O₃ due to the assimilation is much larger than the O₃ sensitivities to the EAS
817 anthropogenic emissions, the assimilation mainly improved the contributions from other sources,
818 possibly including the stratospheric O₃.

819
820 The quality of the model boundary conditions only indicates how well the total “transported
821 background” component is represented, and can not be directly connected with the accuracy of the
822 model estimated R(O₃, EAS, 20%) sensitivities, which also show notable intermodel differences:
823 The estimated R(MDA8, EAS, 20%) in the different STEM cases range from <1.0 ppbv to ~1.3
824 ppbv, at least 40% higher than the May-June period mean in Figures 10-11. The mean R(MDA8,
825 EAS, 20%) at three high O₃ CASTNET sites range from 0.73 (STEM/GEOS-Chem) to 0.98 ppbv
826 (STEM/C-IFS), with the mean S_{O₃} of ~1.14 at these sites based on the STEM/RAQMS runs due
827 to the nonlinear emission perturbation-O₃ response relationships (Figure 15e-h). The R(MDA8,
828 EAS, 100%) from the STEM/RAQMS case is as high as >7 ppbv over the high terrain regions.
829 These are of smaller magnitudes than the estimates in Lin et al. (2012a), possibly due to the
830 differences in the used models and the bottom-up emission inputs.

831
832 A stratospheric O₃ intrusion also affected the Northeast US on the same day, as revealed
833 by the satellite mid- tropospheric O₃ and CO observations (Figure 13). This intrusion was mixed
834 with LRT East Asian pollution (Figure 15 and Figure S5). However, this intrusion did not enhance
835 the NE boundary layer/surface O₃ concentrations, which were actually anomalously low
836 (MDA8<40 ppbv) as indicated by the model base simulations and the CASTNET observations
837 (Figure 15a-d). Similar characteristics during summertime stratospheric O₃ intrusion events
838 around this region have been discussed by Ott et al. (2016). The East Asian pollution less intensely
839 (<50%) affected the surface O₃ levels in these regions than in the US west, due to the greater
840 transport distances, stronger local emission influence on chemical production/loss, shallower
841 PBLHs, as well as the impact of the overall flat terrain in the US east.

842
843 A summertime LRT event on 9-10 June is analyzed to contrast with the 9 May case study.
844 Lin et al. (2012b) showed that >80 ppbv of ozonesonde data in northern California at 2-6 km

845 measured the stratospheric O₃ remnants during this episode, and the transported stratospheric O₃
846 contributed to as much as ~50% of the total O₃ in southern California based on their model
847 calculations. We show that on 10 June over 100 ppbv of O₃, as well as <90 ppbv CO, was observed
848 by satellites at ~500 hPa above Nevada and northern California (Figure 16), which again was
849 substantially underestimated by all free-running models (Figure 17), resulting in the
850 underpredicted total O₃ at two CASTNET sites in southern California (Converse Station and
851 Joshua Tree NP) that experienced O₃ exceedances on this day (Figure 18a-c). The negative biases
852 in the “transported background” O₃ and surface MDA8 O₃ were successfully reduced by
853 incorporating satellite data (Figures 17 and 18d).

854
855 Figures 18e-h show that LRT of EAS anthropogenic pollution also strongly affected
856 southern California and Nevada. Notable intermodel differences are again found in the estimated
857 R(MDA8, EAS, 20%), but they are overall lower than on 9 May (<1.0 ppbv). The mean R(MDA8,
858 EAS, 20%) at the two high O₃ CASTNET sites range from 0.54 (STEM/C-IFS) to 0.86 ppbv
859 (STEM/RAQMS), with the mean S_{O₃} of ~1.13 at these sites based on the STEM/RAQMS runs
860 (Figure 18e-h). The R(MDA8, EAS, 100%) from the STEM/RAQMS case is as high as >6 ppbv
861 over southern California and Nevada. Compared to the spring event, R(MDA8, EAS, 20%) in the
862 eastern US are discernable only over a limited region, due to weaker transport and stronger local
863 chemical production/loss.

864 865 **4. Conclusions and suggestions on future directions**

866
867 In support of the HTAP Phase 2 experiment that involved high-resolution global models
868 and regional models’ participation to advance the understanding of the pollutants’ SR relationships
869 in the Northern Hemisphere, we conducted a number of regional scale STEM base and forward
870 sensitivity simulations over NAM during May-June 2010. STEM’s top and lateral chemical
871 boundary conditions were downscaled from three global models’ (i.e., GEOS-Chem, RAQMS,
872 and ECMWF C-IFS) base and sensitivity simulations (in which the East Asian anthropogenic
873 emissions were reduced by 20%). Despite dilution along the great transport distance, the East
874 Asian anthropogenic sources still had distinguishable impact on the NAM surface O₃, with the
875 period-mean NAM O₃ sensitivities to a 20% reduction of the East Asian anthropogenic emissions
876 (i.e., R(O₃, EAS, 20%)) ranging from ~0.24 ppbv (STEM/C-IFS) to ~0.34 ppbv (STEM/RAQMS).
877 The spatial patterns of the STEM surface O₃ sensitivities over NAM overall resembled those from
878 its corresponding boundary condition model, with regional/period mean R(O₃, EAS, 20%) differed
879 slightly (<10%) from its corresponding boundary condition model’s, which are smaller than those
880 among its boundary condition models. The boundary condition models’ two-month mean R(O₃,
881 EAS, 20%) was ~8% lower than the mean sensitivity estimated by eight global models. Therefore,
882 choosing other global model outputs as STEM’s boundary conditions may lead to different STEM
883 O₃ sensitivities. The biases and RMSEs in the simulated total O₃, which differed significantly
884 among models, can partially be due to the uncertainty in the bottom-up NO_x emission inputs
885 according to the model comparison with the OMI NO₂ columns, and future work on attributing the
886 intermodel differences on process level is particularly important for better understanding the
887 sources of uncertainties in the modeled total O₃ and its source contribution.

888
889 The HTAP2 multi-model ensemble mean R(O₃, EAS, 20%) values in 2010 were higher
890 than the HTAP1 reported 2001 conditions, due to a number of reasons including the impacts of

891 the growing East Asian anthropogenic emissions, the interannual variability in atmospheric
892 circulation (i.e., stronger trans-Pacific transport in spring 2010 following an El Niño event), and
893 the different experiment designs of HTAP1 and HTAP2. The GEOS-Chem O₃ sensitivities in 2010
894 were also higher than the 2008-2009 conditions due to the increasing Asian emissions and the
895 spring 2010 meteorological conditions that favored the trans-Pacific pollution transport. The
896 GEOS-Chem sensitivity calculations indicate that the East Asian anthropogenic NO_x emissions
897 mattered more than the other East Asian O₃ precursors to the NAM O₃, qualitatively consistent
898 with previous adjoint sensitivity calculations. Continued research is needed on temporal changes
899 of emissions for different species and sectors in NAM and foreign countries as well as their impacts
900 on the SR relationships. As emissions from various source sectors can differ by emitted altitudes
901 and temporal profiles, efforts should also be placed to have the models timely update the height
902 and temporal profiles of the emissions from various sectors.

903
904 An additional STEM simulation was performed in which the boundary conditions were
905 downscaled from a RAQMS simulation without East Asian anthropogenic emissions (i.e., a 100%
906 emission reduction), to assess the scalability of the mean O₃ sensitivities to the size of the emission
907 perturbation. The scalability was found to be spatially varying, ranging from 1.15-1.25 for column
908 O₃ in most US regions, which were overall ~0.05 higher than the surface O₃'s. Therefore, the full
909 source contribution obtained by linearly scaling the NAM regional mean O₃ sensitivity to the 20%
910 reduction in the East Asian emissions may be underestimated by at least 10%. The underestimation
911 in other seasons of the HTAP2 study period may be higher and will need to be quantified in future
912 work. Also, motivated by Lapina et al. (2014), additional calculations will be conducted in future
913 to explore the scalability of different O₃ metrics in these cases. For future source attribution
914 analysis, in general it is recommended to directly choose the suitable size of the emission
915 perturbation based on the specific questions to address, and to avoid linearly scaling O₃
916 sensitivities that are based on other amounts of the perturbations.

917
918 The STEM O₃ sensitivities to the East Asian anthropogenic emissions (based on three
919 boundary condition models separately and averagely) were strong during 3-6 episodes in May-
920 June 2010, following similar diurnal cycles as the total O₃. Stronger East Asian anthropogenic
921 pollution impacts were estimated during the observed O₃ exceedances in the western US than on
922 all days, especially over the high terrain rural/remote areas; in contrast, the East Asian
923 anthropogenic pollution impacts were less strong during O₃ exceedances in other US regions. We
924 emphasized the importance of saving model results hourly for conveniently calculating policy-
925 relevant metrics, as well as the usefulness of hourly sampling frequency of the planned
926 geostationary satellites for better evaluating the impacts of the LRT events.

927
928 Based on model calculations, satellite O₃ (TES, JPL-IASI, and AIRS), CO (TES and AIRS)
929 and surface O₃ observations on 9 May 2010, we showed the different influences from stratospheric
930 O₃ intrusions along with the transported East Asian pollution on O₃ in the western and the eastern
931 US. This event was further compared with a summer event of 10 June 2010. During both events,
932 the unsatisfactory performance of free-running (i.e., without chemical data assimilation) global
933 models would pose difficulties for regional models (regardless of their resolutions and other
934 configurations, parameterization) to accurately simulate the surface O₃ and its source contribution
935 using boundary conditions downscaled from these model runs. Incorporating satellite (OMI and
936 MLS) O₃ data effectively improved the modeled O₃. As chemical data assimilation techniques

937 keep developing (Bocquet et al., 2015), several HTAP2 participating global models have already
938 been able to assimilate single- or multi- constitute satellite atmospheric composition data (e.g.,
939 Miyazaki et al., 2012; Parrington et al., 2008, 2009; Huang et al., 2015; Inness et al., 2015;
940 Flemming et al., 2017). Comparing the performance of the assimilated fields from different models,
941 and making the global model assimilated chemical fields in the suitable format for being used as
942 boundary conditions would be very beneficial for future regional modeling, as well as for better
943 interpreting the pollutants' distributions especially during the exceptional events. Meanwhile,
944 efforts should also be devoted to advancing and applying higher-resolution regional scale
945 modeling and chemical data assimilation. Furthermore, although satellite observations have been
946 applied for improving the estimated US background O₃ (e.g., Huang et al., 2015), using satellite
947 (and/or other types of) observations to improve SR relationship studies also needs to be explored.
948 Some of the possible methods include: 1) The combination of data assimilation and the tagging
949 approach; 2) Introducing observation-constrained emission estimates in the emission perturbation
950 analyses.

951

952 **Acknowledgements**

953

954 The global and regional modeling results used in this study have been submitted to the
955 AeroCom database following the HTAP2 data submission guidelines ([http://iek8wikis.iek.fz-](http://iek8wikis.iek.fz-juelich.de/HTAPWiki/HTAP-2-data-submission)
956 [juelich.de/HTAPWiki/HTAP-2-data-submission](http://iek8wikis.iek.fz-juelich.de/HTAPWiki/HTAP-2-data-submission)), or can be made available upon request.
957 Technical support from Anna Carlin Benedictow, Brigitte Koffi, Jan Griesfeller, and Michael
958 Schulz regarding formatting and submitting the data to the AeroCom is acknowledged. MH thanks
959 the research resources at the University of Iowa and JPL/Caltech that supported this study, as well
960 as the travel funding from the US EPA for attending the related HTAP2 workshops. DKH and YD
961 recognize support from NASA ACAST. FD Acknowledges support from the Administrative
962 Arrangement. Part of this research was carried out at the Jet Propulsion Laboratory, California
963 Institute of Technology, under contract to the National Aeronautics and Space Administration.
964 Reference herein to any specific commercial product, process or service by trade name, trademark,
965 manufacturer or otherwise does not constitute or imply its endorsement by the United States
966 Government or the Jet Propulsion Laboratory, California Institute of Technology. The views,
967 opinions, and findings contained in this report are those of the author(s) and should not be
968 construed as an official National Oceanic and Atmospheric Administration or U.S. Government
969 position, policy, or decision. We also acknowledge the feedbacks from Dr. Gail Tonnesen, two
970 anonymous reviewers, and Dr. Meiyun Lin on earlier versions of this paper, that helped improve
971 its quality.

972

973 **References**

974

975 Anderson, D. C., Loughner, C. P., Diskin, G., Weinheimer, A., Canty, T., P., Salawitch, R. J.,
976 Worden, H. M., Fried, A., 25 Mikoviny, T., Wisthaler, A., and Dickerson, R., R. (2014),
977 Measured and modeled CO and NO_v in DISCOVER-AQ: An evaluation of emissions and
978 chemistry over the eastern US, *Atmos. Environ.*, 96, 78-87, doi:
979 10.1016/j.atmosenv.2014.07.004.

980 Allen, D. J., Pickering, K. E., Pinder, R. W., Henderson, B. H., Appel, K. W., and Prados, A.
 981 (2012), Impact of lightning-NO on eastern United States photochemistry during the summer
 982 of 2006 as determined using the CMAQ model, *Atmos. Chem. Phys.*, 12, 1737-1758, doi:
 983 10.5194/acp-12-1737-2012.

984 Ambrose, J.L., Reidmiller, D.R., and Jaffe, D.A. (2011), Causes of high O₃ in the lower free
 985 troposphere over the Pacific Northwest as observed at the Mt. Bachelor Observatory. *Atmos.*
 986 *Environ.*, 45, 5302–5315, doi: 10.1016/j.atmosenv.2011.06.056.

987 Anenberg, S. C., L. W. Horowitz, D. Q. Tong, and J. J. West (2010), An estimate of the global
 988 burden of anthropogenic ozone and fine particulate matter on premature human mortality using
 989 atmospheric modeling, *Environ. Health Perspect.*, 118(9), 1189–1195.

990 Avnery, S, D.L. Mauzerall, J. Liu, L.W. Horowitz (2011a), Global Crop Yield Reductions due to
 991 Surface Ozone Exposure: 1. Year 2000 Crop Production Losses and Economic
 992 Damage, *Atmos. Environ.*, 45, 2284-2296.

993 Avnery, S, D.L. Mauzerall, J. Liu, L.W. Horowitz (2011b), Global Crop Yield Reductions due to
 994 Surface Ozone Exposure: 2. Year 2030 Potential Crop Production Losses and Economic
 995 Damage under Two Scenarios of O₃ Pollution, *Atmos. Environ.*, 45, 2297-2309.

996 Beer, R., T. A. Glavich, and D. M. Rider (2001), Tropospheric emission spectrometer for the Earth
 997 Observing System's Aura satellite, *Applied Optics*, 40, 2356 – 2367.

998 Beer, R (2006), TES on the Aura Mission: Scientific Objectives, Measurements, and Analysis
 999 Overview, *IEEE Transaction on Geoscience and Remote Sensing*, 44, 1102-1105.

1000 Bian, J., A. Gettelman, H. Chen, and L. L. Pan (2007), Validation of satellite ozone profile
 1001 retrievals using Beijing ozonesonde data, *J. Geophys. Res.*, 112, D06305,
 1002 doi:10.1029/2006JD007502.

1003 Bocquet, M., Elbern, H., Eskes, H., Hirtl, M., Žabkar, R., Carmichael, G. R., Flemming, J., Inness,
 1004 A., Pagowski, M., Pérez Camaño, J. L., Saide, P. E., San Jose, R., Sofiev, M., Vira, J.,
 1005 Baklanov, A., Carnevale, C., Grell, G., and Seigneur, C. (2015), Data assimilation in
 1006 atmospheric chemistry models: current status and future prospects for coupled chemistry
 1007 meteorology models, *Atmos. Chem. Phys.*, 15, 5325-5358, doi:10.5194/acp-15-5325-2015.

1008 Boersma, K. F., Braak, R., van der A, R. J. (2011a), Dutch OMI NO₂ (DOMINO) data product
 1009 v2.0 HE5 data file user manual. http://www.temis.nl/docs/OMI_NO2_HE5_2.0_2011.pdf.

1010 Boersma, K. F., Eskes, H. J., Dirksen, R. J., van der A, R. J., Veefkind, J. P., Stammes, P., Huijnen,
 1011 V., Kleipool, Q. L., Sneep, M., Claas, J., Leitão, J., Richter, A., Zhou, Y., Brunner, D. (2011b),
 1012 An improved tropospheric NO₂ column retrieval algorithm for the Ozone Monitoring
 1013 Instrument, *Atmos. Meas. Tech.*, 4, 1905-1928.

1014 Bowman, K. W., Rodgers, C. D., Kulawik, S. S., Worden, J., Sarkissian, E., Osterman, G., Steck,
 1015 T., Lou, M., Eldering, A., Shephard, M., Worden, H., Lampel, M., Clough, S., Brown, P.,
 1016 Rinsland, C., Gunson, M., and Beer, R. (2006), Tropospheric Emission Spectrometer:
 1017 Retrieval method and error analysis, *IEEE Transaction on Geoscience and Remote Sensing*,
 1018 44 (5), 1297–1307, doi: 10.1109/TGRS.2006.871234.

1019 Bowman, K., and D. K. Henze (2012), Attribution of direct ozone radiative forcing to spatially
 1020 resolved emissions, *Geophys. Res. Lett.*, 39, L22704, doi:10.1029/2012GL053274.

1021 Brioude, J., Angevine, W. M., Ahmadov, R., Kim, S.-W., Evan, S., McKeen, S. A., Hsie, E.-Y.,
1022 Frost, G. J., Neuman, J. A., Pollack, I. B., Peischl, J., Ryerson, T. B., Holloway, J., Brown, S.
1023 S., Nowak, J. B., Roberts, J. M., Wofsy, S. C., Santoni, G. W., Oda, T., and Trainer, M. (2013),
1024 Top-down estimate of surface flux in the Los Angeles Basin using a mesoscale inverse
1025 modeling technique: assessing anthropogenic emissions of CO, NO_x and CO₂ and their
1026 impacts, *Atmos. Chem. Phys.*, 13, 3661-3677, doi:10.5194/acp-13-3661-2013.

1027 Brown-Steiner, B., and P. Hess (2011), Asian influence on surface ozone in the United States: A
1028 comparison of chemistry, seasonality, and transport mechanisms, *J. Geophys. Res.*, 116,
1029 D17309, doi:10.1029/2011JD015846.

1030 Cai, C., J. T. Kelly, J. C. Avise, A. P. Kaduwela, and W. R. Stockwell (2011), Photochemical
1031 Modeling in California with Two Chemical Mechanisms: Model Intercomparison and
1032 Response to Emission Reductions, *J. Air & Waste Manage. Assoc.*, 61:5, 559-572, doi:
1033 10.3155/1047-3289.61.5.559.

1034 Canty, T. P., Hembeck, L., Vinciguerra, T. P., Anderson, D. C., Goldberg, D. L., Carpenter, S. F.,
1035 Allen, D. J., Loughner, C. P., Salawitch, R. J., and Dickerson, R. R. (2015), Ozone and NO_x
1036 chemistry in the eastern US: evaluation of CMAQ/CB05 with satellite (OMI) data, *Atmos.*
1037 *Chem. Phys.*, 15, 10965-10982, doi:10.5194/acp-15-10965-2015.

1038 Carmichael, G.R., Tang, Y., Kurata, G., Uno, I., Streets, D.G., Thongboonchoo, N., Woo, J.H.,
1039 Guttikunda, S., White, A., Wang, T., Blake, D.R., Atlas, E., Fried, A., Potter, B., Avery, M.A.,
1040 Sachse, G.W., Sandholm, S.T., Kondo, Y., Talbot, R.W., Bandy, A., Thornton, D., and Clarke,
1041 A.D. (2003a), Evaluating regional emission estimates using the TRACE-P observations, *J.*
1042 *Geophys. Res.*, 108 (D21), 8810, doi: 10.1029/2002JD003116.

1043 Carmichael, G.R., Tang, Y., Kurata, G., Uno, I., Streets, D., Woo, J.H., Huang, H., Yienger, J.,
1044 Lefer, B., Shetter, R., Blake, D., Atlas, E., Fried, A., Apel, E., Eisele, F., Cantrell, C., Avery,
1045 M., Barrick, J., Sachse, G., Brune, W., Sandholm, S., Kondo, Y., Singh, H., Talbot, R., Bandy,
1046 A., Thornton, D., Clarke, A., and Heikes, B. (2003b), Regional-scale chemical transport
1047 modeling in support of the analysis of observations obtained during the TRACE-P experiment,
1048 *J. Geophys. Res.*, 108 (D21), 8823, doi: 10.1029/2002JD003117.

1049 Carter, W. P. L. (2000), Documentation of the SAPRC-99 chemical mechanism for VOC
1050 Reactivity Assessment, final report to California Air Resources Board, Contract No. 92-329
1051 and 95-308.

1052 Cooper, O. R., et al. (2010), Increasing springtime ozone mixing ratios in the free troposphere over
1053 western North America, *Nature*, 463, doi: 10.1038/nature08708.

1054 Cooper, O. R., Oltmans, S. J., Johnson, B. J., Brioude, J., Angevine, W., Trainer, M., Parrish, D.
1055 D., Ryerson, T. R., Pollack, I., Cullis, P. D., Ives, M. A., Tarasick, D. W., Al-Saadi, J., and
1056 Stajner, I. (2011), Measurement of western U.S. baseline ozone from the surface to the
1057 tropopause and assessment of downwind impact regions, *J. Geophys. Res.*, 116, D00V03, doi:
1058 10.1029/2011JD016095.

1059 Cooper, O., et al. (2016), Western NA Performance Evaluation for HTAP2, HTAP2 workshop,
1060 Potsdam, Germany, 2016.

1061 Crippa, M., Janssens-Maenhout, G., Dentener, F., Guizzardi, D., Sindelarova, K., Muntean, M.,
1062 Van Dingenen, R., and Granier, C. (2016), Forty years of improvements in European air
1063 quality: regional policy-industry interactions with global impacts, *Atmos. Chem. Phys.*, 16,
1064 3825-3841, doi:10.5194/acp-16-3825-2016.

1065 Emmons, L. K., Hess, P. G., Lamarque, J.-F., and Pfister, G. G. (2012), Tagged ozone mechanism
1066 for MOZART-4, CAM-chem and other chemical transport models, *Geosci. Model Dev.*, 5,
1067 1531-1542, doi:10.5194/gmd-5-1531-2012.

1068 Eskes, H. J. and Boersma, K. F. (2003), Averaging kernels for DOAS total-column satellite
1069 retrievals, *Atmos. Chem. Phys.*, 3, 1285-1291.

1070 Fiore, A. M., et al. (2009), Multimodel estimates of intercontinental source receptor relationships
1071 for ozone pollution, *J. Geophys. Res.*, 114, D04301, doi:10.1029/2008JD010816.

1072 Fiore, A. M., J. T. Oberman, M. Y. Lin, L. Zhang, O. E. Clifton, D. J. Jacob, V. Naik, L. W.
1073 Horowitz, J. P. Pinto, and G. P. Milly (2014), Estimating North American background ozone
1074 in U.S. surface air with two independent global models: Variability, uncertainties, and
1075 recommendations, *Atmos. Environ.*, 96, 284–300, doi: 10.1016/j.atmosenv.2014.07.045.

1076 Flemming, J., Huijnen, V., Arteta, J., Bechtold, P., Beljaars, A., Blechschmidt, A.-M., Diamantakis,
1077 M., Engelen, R. J., Gaudel, A., Inness, A., Jones, L., Josse, B., Katragkou, E., Marecal, V.,
1078 Peuch, V.-H., Richter, A., Schultz, M. G., Stein, O., and Tsikerdekis, A. (2015), Tropospheric
1079 chemistry in the Integrated Forecasting System of ECMWF, *Geosci. Model Dev.*, 8, 975-1003,
1080 doi:10.5194/gmd-8-975-2015.

1081 Flemming, J., Benedetti, A., Inness, A., Engelen, R., Jones, L., Huijnen, V., Remy, S., Parrington,
1082 M., Suttie, M., Bozzo, A., Peuch, V.-H., Akritidis, D., and Katragkou, E. (2017), The CAMS
1083 interim Reanalysis of Carbon Monoxide, Ozone and Aerosol for 2003–2015, *Atmos. Chem.*
1084 *Phys.*, 17, 1945-1983, doi:10.5194/acp-17-1945-2017.

1085 Galmarini, S., C. Hogrefe, D. Brunner, P. Makar, A. Baklanov (2015), Preface to the AQMEII p2
1086 Special issue, *Atmos. Environ.*, 115, 340-344.

1087 Galmarini, S., Koffi, B., Solazzo, E., Keating, T., Hogrefe, C., Schulz, M., Benedictow, A.,
1088 Griesfeller, J. J., Janssens-Maenhout, G., Carmichael, G., Fu, J., and Dentener, F. (2017),
1089 Technical note: Coordination and harmonization of the multi-scale, multi-model activities
1090 HTAP2, AQMEII3, and MICS-Asia3: simulations, emission inventories, boundary conditions,
1091 and model output formats, *Atmos. Chem. Phys.*, 17, 1543-1555, doi:10.5194/acp-17-1543-
1092 2017.

1093 Geddes, J. A., Heald, C. L., Silva, S. J., and Martin, R. V. (2016), Land cover change impacts on
1094 atmospheric chemistry: simulating projected large-scale tree mortality in the United States,
1095 *Atmos. Chem. Phys.*, 16, 2323-2340, doi:10.5194/acp-16-2323-2016.

1096 Gery, M. W., G. Z. Whitten, J. P. Killus, and M. C. Dodge (1989), A photochemical kinetics
1097 mechanism for urban and regional scale computer modeling, *J. Geophys. Res.*, 94, 12,925 –
1098 12,956, doi:10.1029/JD094iD10p12925.

1099 Granier, C., Lamarque, J. F., Mieville, A., Muller, J. F., Olivier, J., Orlando, J., Peters, J., Petron,
1100 G., Tyndall, G., and Wallens, S. (2005), POET, a database of surface emissions of ozone
1101 precursors, <http://www.aero.jussieu.fr/projet/ACCENT/POET.php>.

1102 Gratz, L.E., Jaffe, D.A., and Hee, J.R. (2014), Causes of increasing ozone and decreasing carbon
1103 monoxide in springtime at the Mt. Bachelor Observatory from 2004 to 2013, *Atmos. Environ.*,
1104 109, 323–330, doi: 10.1016/j.atmosenv.2014.05.076.

1105 Guenther, A. B., X. Jiang, C. L. Heald, T. Sakulyanontvittaya, T. Duhl, L. K. Emmons, and X.
1106 Wang (2012), The Model of Emissions of Gases and Aerosols from Nature version 2.1
1107 (MEGAN2.1): an extended and updated framework for modeling biogenic emissions, *Geosci.*
1108 *Model Dev.*, 5 (6), 1471-1492.

1109 Henze, D. K., Hakami, A., and Seinfeld, J. H. (2007), Development of the adjoint of GEOS-Chem,
1110 *Atmos. Chem. Phys.*, 7, 2413–2433, doi:10.5194/acp-7-2413-2007.

1111 Hilsenrath, E., and K. Chance (2013), NASA ups the TEMPO on monitoring air pollution, *Earth*
1112 *Obs.*, 25, 10–15.

1113 Hogrefe, C., Isukapalli, S., Tang, X., Georgopoulos, P., He, S., Zalewsky, E., Hao, W., Ku, J.,
1114 Key, T., and Sistla, G. (2011), Impact of biogenic emission uncertainties on the simulated
1115 response of ozone and fine Particulate Matter to anthropogenic emission reductions, *J. Air*
1116 *Waste Manage.*, 61, 92–108.

1117 Huang, M., Carmichael, G. R., Adhikary, B., Spak, S. N., Kulkarni, S., Cheng, Y. F., Wei, C.,
1118 Tang, Y., Parrish, D. D., Oltmans, S. J., D'Allura, A., Kaduwela, A., Cai, C.,
1119 Weinheimer, A. J., Wong, M., Pierce, R. B., Al-Saadi, J. A., Streets, D. G., and Zhang, Q.
1120 (2010), Impacts of transported background ozone on California air quality during the
1121 ARCTAS-CARB period – a multi-scale modeling study, *Atmos. Chem. Phys.*, 10, 6947-6968,
1122 doi: 10.5194/acp-10-6947-2010.

1123 Huang, M., Carmichael, G. R., Chai, T., Pierce, R. B., Oltmans, S. J., Jaffe, D. A.,
1124 Bowman, K. W., Kaduwela, A., Cai, C., Spak, S. N., Weinheimer, A. J., Huey, L. G., and
1125 Diskin, G. S. (2013a), Impacts of transported background pollutants on summertime western
1126 US air quality: model evaluation, sensitivity analysis and data assimilation, *Atmos. Chem.*
1127 *Phys.*, 13, 359-391, doi: 10.5194/acp-13-359-2013.

1128 Huang, M., Bowman, K. W., Carmichael, G. R., Pierce, R. B., Worden, H. M., Luo, M., Cooper,
1129 O. R., Pollack, I. B., Ryerson, T. B., Brown, S. S. (2013b), Impact of southern California
1130 anthropogenic emissions on ozone pollution in the mountain states, *J. Geophys. Res.*, 118,
1131 12784-12803, doi: 10.1002/2013JD020205.

1132 Huang, M., et al. (2014), Changes in nitrogen oxides emissions in California during 2005–2010
1133 indicated from top-down and bottom-up emission estimates, *J. Geophys. Res.*, 119, 12,928–
1134 12,952, doi: 10.1002/2014JD022268, 2014.

1135 Huang, M., et al. (2015), Improved Western US Background Ozone Estimates via Constraining
1136 Nonlocal and Local Source Contributions using Aura TES and OMI Observations, *J. Geophys.*
1137 *Res.*, 120, 3572–3592, doi: 10.1002/2014JD022993.

1138 Huang, M., Carmichael, G. R., Crawford, J. H., Wisthaler, A., Zhan, X., Hain, C. R., Lee, P., and
1139 Guenther, A. B. (2017), Linkages between land initialization of the NASA-Unified WRF v7
1140 and biogenic isoprene emission estimates during the SEAC4RS and DISCOVER-AQ airborne
1141 campaigns, *Geosci. Model Dev. Discuss.*, doi:10.5194/gmd-2017-13, in review.

1142 Inness, A., Blechschmidt, A.-M., Bouarar, I., Chabrillat, S., Crepulja, M., Engelen, R. J., Eskes,
1143 H., Flemming, J., Gaudel, A., Hendrick, F., Huijnen, V., Jones, L., Kapsomenakis, J.,
1144 Katragkou, E., Keppens, A., Langerock, B., de Mazière, M., Melas, D., Parrington, M., Peuch,
1145 V. H., Razinger, M., Richter, A., Schultz, M. G., Suttie, M., Thouret, V., Vrekoussis, M.,
1146 Wagner, A., and Zerefos, C. (2015), Data assimilation of satellite-retrieved ozone, carbon
1147 monoxide and nitrogen dioxide with ECMWF's Composition-IFS, *Atmos. Chem. Phys.*, 15,
1148 5275-5303, doi:10.5194/acp-15-5275-2015.

1149 Jaffe, D.A. (2011), Relationship between surface and free tropospheric ozone in the Western U.S.,
1150 *Environ. Sci. Technol.*, 45, 432–438, doi: 10.1021/es1028102.

1151 Janssens-Maenhout, G., Crippa, M., Guizzardi, D., Dentener, F., Muntean, M., Pouliot, G.,
1152 Keating, T., Zhang, Q., Kurokawa, J., Wankmüller, R., Denier van der Gon, H., Kuenen, J. J.
1153 P., Klimont, Z., Frost, G., Darras, S., Koffi, B., and Li, M. (2015), HTAP_v2.2: a mosaic of
1154 regional and global emission grid maps for 2008 and 2010 to study hemispheric transport of
1155 air pollution, *Atmos. Chem. Phys.*, 15, 11411-11432, doi:10.5194/acp-15-11411-2015.

1156 Jacob, D. J., Logan, J. A., and Murti, P. P. (1999), Effect of rising Asian emissions on surface
1157 ozone in the United States, *Geophys. Res. Lett.*, 26, 2175-2178, doi: 10.1029/1999GL900450.

1158 Jerret, M., R. T. Burnett, C. A. Popo, III, K. Ito, G. Thurston, D. Krewski, Y. Shi, E. Calle, and M.
1159 Thun (2009), Long-Term Ozone Exposure and Mortality, the *New England Journal of*
1160 *Medicine*, 360, 1085-1096, doi: 10.1056/NEJMoa0803894.

1161 Kaiser, J. W., Heil, A., Andreae, M. O., Benedetti, A., Chubarova, N., Jones, L., Morcrette, J.-J.,
1162 Razinger, M., Schultz, M. G., Suttie, M., and van der Werf, G. R. (2012), Biomass burning
1163 emissions estimated with a global fire assimilation system based on observed fire radiative
1164 power, *Biogeosciences*, 9, 527–554, doi:10.5194/bg-9-527-2012.

1165 Kalnay, E., and Co-authors (1996), The NCEP/NCAR 40-Year Reanalysis Project, *Bulletin of the*
1166 *American Meteorological Society*, 77, 437–471.

1167 Kim, S.-W., B. C. McDonald, S. Baidar, S. S. Brown, B. Dube, R. A. Ferrare, G. J. Frost, R. A.
1168 Harley, J. S. Holloway, H.-J. Lee, et al. (2016), Modeling the weekly cycle of NO_x and CO
1169 emissions and their impacts on O₃ in the Los Angeles-South Coast Air Basin during the CalNex
1170 2010 field campaign, *J. Geophys. Res. Atmos.*, 121, 1340–1360, doi:10.1002/2015JD024292.

1171 Koffi, B., Dentener, F., Janssens-Maenhout, G., Guizzardi, D., Crippa, M., Diehl, T., Galmarini,
1172 S., and Solazzo, E.: Hemispheric Transport Air Pollution (HTAP): Specification of the HTAP2
1173 experiments – Ensuring harmonized modelling, EUR 28255 EN – Scientific and Technical
1174 Research Reports, doi:10.2788/725244, 2016.

1175 Langford, A. O., Brioude, J., Cooper, O.R., Senff, C.J., Alvarez II, R.J., Hardesty, R.M., Johnson,
1176 B.J., and Oltmans, S.J. (2011), Stratospheric influence on surface ozone in the Los Angeles
1177 area during late spring and early summer of 2010, *J. Geophys. Res. Atmos.*, 117, D00V06, doi:
1178 10.1029/2011JD016766.

1179 Lapina, K., D. K. Henze, J. B. Milford, M. Huang, M. Lin, A. M. Fiore, G. Carmichael, G. G.
1180 Pfister, and K. Bowman (2014), Assessment of source contributions to seasonal vegetative
1181 exposure to ozone in the U.S., *J. Geophys. Res. Atmos.*, 119, 324–340,
1182 doi:10.1002/2013JD020905.

1183 Levelt, P.F., E. Hilsenrath, G.W. Leppelmeier, G.H.J. van den Oord, P.K. Bhartia, J. Tamminen,
1184 J.F. de Haan and J.P. Veefkind (2006), Science Objectives of the Ozone Monitoring Instrument,
1185 *IEEE Transaction on Geoscience and Remote Sensing*, 44, 1199-1208.

1186 Li, M., Zhang, Q., Kurokawa, J.-I., Woo, J.-H., He, K., Lu, Z., Ohara, T., Song, Y., Streets, D. G.,
1187 Carmichael, G. R., Cheng, Y., Hong, C., Huo, H., Jiang, X., Kang, S., Liu, F., Su, H., and
1188 Zheng, B. (2017), MIX: a mosaic Asian anthropogenic emission inventory under the
1189 international collaboration framework of the MICS-Asia and HTAP, *Atmos. Chem. Phys.*, 17,
1190 935-963, doi:10.5194/acp-17-935-2017.

1191 Lin, M., Holloway, T., Carmichael, G. R., and Fiore, A. M. (2010), Quantifying pollution inflow
1192 and outflow over East Asia in spring with regional and global models, *Atmos. Chem. Phys.*,
1193 10, 4221-4239, doi:10.5194/acp-10-4221-2010.

1194 Lin, M., A. M. Fiore, L. W. Horowitz, O. R. Cooper, V. Naik, J. Holloway, B. J. Johnson, A.
1195 Middlebrook, S. J. Oltmans, I. B. Pollack, T. B. Ryerson, J. X. Warner, C. Wiedinmyer, J.
1196 Wilson, B. Wyman (2012a), Transport of Asian ozone pollution into surface air over the
1197 western United States in spring, *J. Geophys. Res.*, 117, D00V07, doi: 10.1029/2011JD016961.

1198 Lin, M., A. Fiore, O. R. R. Cooper, L. W. Horowitz, A. O. O. Langford, H. Levy II, B. J. Johnson,
1199 V. Naik, S. J. Oltmans, and C. J. Senff (2012b), Springtime high surface ozone events over the
1200 western United States: Quantifying the role of stratospheric intrusions, *J. Geophys. Res.*, 117,
1201 D00V22, doi: 10.1029/2012JD018151.

1202 Lin, M., L.W. Horowitz, S. J. Oltmans, A. M. Fiore, S. Fan (2014), Tropospheric ozone trends at
1203 Manna Loa Observatory tied to decadal climate variability, *Nature Geoscience*, 7, 136-143,
1204 doi:10.1038/NGEO2066.

1205 Lin, M., L. W. Horowitz, O. R. Cooper, D. Tarasick, S. Conley, L. T. Iraci, B. Johnson, T. Leblanc,
1206 I. Petropavlovskikh, and E. L. Yates (2015), Revisiting the evidence of increasing springtime
1207 ozone mixing ratios in the free troposphere over western North America, *Geophys. Res. Lett.*,
1208 42, 8719–8728, doi:10.1002/2015GL065311.

1209 Lin, M., Horowitz, L. W., Payton, R., Fiore, A. M., and Tonnesen, G. (2016), US surface ozone
1210 trends and extremes from 1980–2014: Quantifying the roles of rising Asian emissions,
1211 domestic controls, wildfires, and climate, *Atmos. Chem. Phys. Discuss.*, doi:10.5194/acp-
1212 2016-1093, in review.

1213 Liu, F., Q. Zhang, R. J. van der A, B. Zheng, D. Tong, L. Yan, Y. Zheng, and K. He (2016), Recent
1214 reduction in NO_x emissions over China: Synthesis of satellite observations and emission
1215 inventories, *Environ. Res. Lett.*, 11 (11), 114002, doi: 10.1088/1748-9326/11/11/114002.

1216 Livesey, N.J., M.J. Filipiak, L. Froidevaux, W.G. Read, A. Lambert, M.L. Santee, J.H. Jiang, H.C.
1217 Pumphrey, J.W. Waters, R.E. Cofield, D.T. Cuddy, W.H. Daffer, B.J. Drouin, R.A. Fuller, R.F.
1218 Jarnot, Y.B. Jiang, B.W. Knosp, Q.B. Li, V.S. Perun, M.J. Schwartz, W.V. Snyder, P.C. Stek,
1219 R.P. Thurstans, P.A. Wagner, M. Avery, E.V. Browell, J-P. Cammas, L.E. Christensen, G.S.
1220 Diskin, R-S. Gao, H-J. Jost, M. Loewenstein, J.D. Lopez, P. Nedelec, G.B. Osterman, G.W.
1221 Sachse, and C.R. Webster (2008), Validation of Aura Microwave Limb Sounder O₃ and CO
1222 observations in the upper troposphere and lower stratosphere, *J. Geophys. Res.* 113, D15S02,
1223 doi:10.1029/2007JD008805.

1224 Luecken, D.J., S. Phillips, G. Sarwar, C. Jang, Effects of using the CB05 vs. SAPRC99 vs. CB4
1225 chemical mechanism on model predictions (2008), *Ozone and gas-phase photochemical
1226 precursor concentrations*, *Atmos. Environ.*, 42 (23), 5805-5820, doi:
1227 10.1016/j.atmosenv.2007.08.056.

1228 Maas, R. and P. Grennfelt (eds) (2016), *Towards Cleaner Air Scientific Assessment Report 2016.*
1229 *EMEP Steering Body and Working Group on Effects of the Convention on Long-Range
1230 Transboundary Air Pollution*, Oslo,
1231 [http://www.unece.org/fileadmin/DAM/env/lrtap/ExecutiveBody/35th_session/CLRTAP_Scien
1232 tific_Assessment_Report_-_Final_20-5-2016.pdf](http://www.unece.org/fileadmin/DAM/env/lrtap/ExecutiveBody/35th_session/CLRTAP_Scientific_Assessment_Report_-_Final_20-5-2016.pdf).

1233 Madronich, S., Flocke, S., Zeng, J., Petropavlovskikh, I., and Lee-Taylor, J. (2002), *The
1234 Tropospheric Ultra-violet Visible (TUV) model Manual*,
1235 [https://www2.acom.ucar.edu/modeling/tropospheric-ultraviolet-and-visible-tuv-radiation-
1236 model](https://www2.acom.ucar.edu/modeling/tropospheric-ultraviolet-and-visible-tuv-radiation-model).

1237 Mauzerall, D. L. and Wang, X. (2001), Protecting Agricultural Crops from the Effects of
1238 Tropospheric Ozone Exposure: Reconciling Science and Standard Setting in the United States,
1239 Europe and Asia, *Annual Review of Energy and the Environment*, 26, 237-268.

1240 McDonald-Buller, E. C., et al. (2011), Establishing policy relevant background (PRB) ozone
1241 concentrations in the United States, *Environ. Sci. Technol.*, 45, 9484–9497.

1242 Meijer, E. W., van Velthoven, P. F. J., Brunner, D. W., Huntrieser, H., and Kelder, H. (2001),
1243 Improvement and evaluation of the parameterization of nitrogen oxide production by lightning,
1244 *Phys. Chem. Earth Pt. C*, 26, 577–583.

1245 Mesinger, F., DiMego, G., Kalnay, E., Mitchell, K., Shafran, P. C., Ebisuzaki, W., Jovic, D.,
1246 Woollen, J., Rogers, E., Berbery, E. H., Ek, M. B., Fan, Y., Grumbine, R., Higgins, W., Li, H.,
1247 Lin, Y., Manikin, G., Parrish, D. and Shi, W. (2006), North American Regional Reanalysis,
1248 *Bulletin of the American Meteorological Society*, 87(3), 343–360, doi: 10.1175/BAMS-87-3-
1249 343.

1250 Miyazaki, K., Eskes, H. J., Sudo, K., Takigawa, M., van Weele, M., Boersma, K. F. (2012),
1251 Simultaneous assimilation of satellite NO₂, O₃, CO, and HNO₃ data for the analysis of
1252 tropospheric chemical composition and emissions, *Atmos. Chem. Phys.*, 12, 9545-9579.

1253 Monks, P. S., Archibald, A. T., Colette, A., Cooper, O., Coyle, M., Derwent, R., Fowler, D.,
1254 Granier, C., Law, K. S., Mills, G. E., Stevenson, D. S., Tarasova, O., Thouret, V., von
1255 Schneidmesser, E., Sommariva, R., Wild, O., and Williams, M. L. (2015), Tropospheric
1256 ozone and its precursors from the urban to the global scale from air quality to short-lived
1257 climate forcer, *Atmos. Chem. Phys.*, 15, 8889-8973, doi:10.5194/acp-15-8889-2015.

1258 Murray, L. T., D. J. Jacob, J. A. Logan, R. C. Hudman, and W. J. Koshak (2012), Optimized
1259 regional and interannual variability of lightning in a global chemical transport model
1260 constrained by LIS/OTD satellite data, *J. Geophys. Res.*, 117, D20307,
1261 doi:10.1029/2012JD017934.

1262 National Research Council (NRC) (2009), global sources of local pollution-An Assessment of
1263 Long-Range Transport of Key Air Pollutants to and from the United States, 35-66,
1264 http://books.nap.edu/openbook.php?record_id=12743&page=35.

1265 Neuman, J. A., et al. (2012), Observations of ozone transport from the free troposphere to the Los
1266 Angeles basin, *J. Geophys. Res. Atmos.*, 117, D00V09, doi: 10.1029/2011JD016919.

1267 Oetjen, H., Payne, V. H., Kulawik, S. S., Eldering, A., Worden, J., Edwards, D. P., Francis, G. L.,
1268 Worden, H. M., Clerboux, C., Hadji-Lazaro, J., and Hurtmans, D. (2014), Extending the
1269 satellite data record of tropospheric ozone profiles from Aura-TES to MetOp-IASI:
1270 characterisation of optimal estimation retrievals, *Atmos. Meas. Tech.*, 7, 4223–4236,
1271 doi:10.5194/amt-7-4223-2014.

1272 Oetjen, H., Payne, V. H., Neu, J. L., Kulawik, S. S., Edwards, D. P., Eldering, A., Worden, H. M.,
1273 and Worden, J. R. (2016), A joint data record of tropospheric ozone from Aura-TES and
1274 MetOp-IASI, *Atmos. Chem. Phys.*, 16, 10229-10239, doi:10.5194/acp-16-10229-2016.

1275 Ott, L. E., B. N. Duncan, A. M. Thompson, G. Diskin, Z. Fasnacht, A. O. Langford, M. Lin, A. M.
1276 Molod, J. E. Nielsen, S. E. Pusede, et al. (2016), Frequency and impact of summertime
1277 stratospheric intrusions over Maryland during DISCOVER-AQ (2011): New evidence from
1278 NASA's GEOS-5 simulations, *J. Geophys. Res. Atmos.*, 121, 3687–3706,
1279 doi:10.1002/2015JD024052.

1280 Park, R. J., D. J. Jacob, B. D. Field, R. M. Yantosca, and M. Chin (2004), Natural and
1281 transboundary pollution influences on sulfate-nitrate-ammonium aerosols in the United States:
1282 Implications for policy, *J. Geophys. Res.*, 109, D15204, doi:10.1029/2003JD004473.

1283 Parrington, M., D. B. A. Jones, K. W. Bowman, L. W. Horowitz, A. M. Thompson, D. W. Tarasick,
1284 and J. C. Witte (2008), Estimating the summertime tropospheric ozone distribution over North
1285 America through assimilation of observations from the Tropospheric Emission Spectrometer,
1286 *J. Geophys. Res.*, 113, D18307, doi:10.1029/2007JD009341.

1287 Parrington, M., D. B. A. Jones, K. W. Bowman, A. M. Thompson, D. W. Tarasick, J. Merrill, S.
1288 J. Oltmans, T. Leblanc, J. C. Witte, and D. B. Millet (2009), Impact of the assimilation of
1289 ozone from the Tropospheric Emission Spectrometer on surface ozone across North America,
1290 *Geophys. Res. Lett.*, 36, L04802, doi:10.1029/2008GL036935.

1291 Parrish, D. D., D. B. Millet, and A. H. Goldstein (2009), Increasing ozone in marine boundary
1292 layer inflow at the west coasts of North America and Europe, *Atmos. Chem. Phys.*, 9, 1303–
1293 1323, doi:10.5194/acp-9-1303-2009.

1294 Parrish, D. D., Aikin, K. C., Oltmans, S. J., Johnson, B. J., Ives, M., and Sweeny, C. (2010), Impact
1295 of transported background ozone inflow on summertime air quality in a California ozone
1296 exceedance area, *Atmos. Chem. Phys.*, 10, 10093-10109, doi:10.5194/acp-10-10093-2010.

1297 Parrish, D. D., et al. (2012), Long-term changes in lower tropospheric baseline ozone
1298 concentrations at northern mid-latitudes, *Atmos. Chem. Phys.*, 12, 11,485–11,504,
1299 doi:10.5194/acp-12-11485-2012.

1300 Pierce, R. B., et al. (2007), Chemical data assimilation estimates of continental U.S. ozone and
1301 nitrogen budgets during the Intercontinental Chemical Transport Experiment–North America,
1302 *J. Geophys. Res.*, 112, D12S21, doi:10.1029/2006JD007722.

1303 Pierce, R. B., et al. (2009), Impacts of background ozone production on Houston and Dallas, Texas,
1304 air quality during the Second Texas Air Quality Study field mission, *J. Geophys. Res.*, 114,
1305 D00F09, doi:10.1029/2008JD011337.

1306 Pouliot, G., H. A.C. Denier van der Gon, J. Kuenen, J. Zhang, M. D. Moran, P.A. Makar (2015),
1307 Analysis of the emission inventories and model-ready emission datasets of Europe and North
1308 America for phase 2 of the AQMEII project, *Atmos. Environ.*, 115, 345-360.

1309 Qu, Z., D. K. Henze, S. L. Capps, Y. Wang, X. Xu, J. Wang (2016), Monthly top-down NO_x
1310 emissions for China (2005-2012): a hybrid inversion method and trend analysis, submitted.

1311 Quennehen, B., Raut, J.-C., Law, K. S., Daskalakis, N., Ancellet, G., Clerbaux, C., Kim, S.-W.,
1312 Lund, M. T., Myhre, G., Olivié, D. J. L., Safieddine, S., Skeie, R. B., Thomas, J. L., Tsyro, S.,
1313 Bazureau, A., Bellouin, N., Hu, M., Kanakidou, M., Klimont, Z., Kupiainen, K.,
1314 Myriokefalitakis, S., Quaas, J., Rumbold, S. T., Schulz, M., Cherian, R., Shimizu, A., Wang,
1315 J., Yoon, S.-C., and Zhu, T. (2016), Multi-model evaluation of short-lived pollutant
1316 distributions over east Asia during summer 2008, *Atmos. Chem. Phys.*, 16, 10765-10792,
1317 doi:10.5194/acp-16-10765-2016.

1318 Reidmiller, D. R., Fiore, A. M., Jaffe, D. A., Bergmann, D., Cuvelier, C., Dentener, F. J., Duncan,
1319 B. N., Folberth, G., Gauss, M., Gong, S., Hess, P., Jonson, J. E., Keating, T., Lupu, A., Marmer,
1320 E., Park, R., Schultz, M. G., Shindell, D. T., Szopa, S., Vivanco, M. G., Wild, O., and Zuber,
1321 A. (2009), The influence of foreign vs. North American emissions on surface ozone in the US,
1322 *Atmos. Chem. Phys.*, 9, 5027-5042, doi:10.5194/acp-9-5027-2009.

1323 Rodgers, C. D. (2000), *Inverse Methods for Atmospheric Sounding: Theory and Practice*, World
1324 Sci., Singapore.

1325 Ryerson, T. B., Andrews, A. E., Angevine, W. M., Bates, T. S., Brock, C. A., Cairns, B., Cohen,
1326 R. C., Cooper, O. R., de Gouw, J. A., Fehsenfeld, F. C., Ferrare, R. A., Fischer, M. L., Flagan,
1327 R. C., Goldstein, A. H., Hair, J. W., Hardesty, R. M., Hostetler, C. A., Jimenez, J. L., Langford,
1328 A. O., McCauley, E., McKeen, S. A., Molina, L. T., Nenes, A., Oltmans, S. J., Parrish, D. D.,
1329 Pederson, J. R., Pierce, R. B., Prather, K., Quinn, P. K., Seinfeld, J. H., Senff, C. J., Sorooshian,
1330 A., Stutz, J., Surratt, J. D., Trainer, M., Volkamer, R., Williams, E. J., Wofsy, S. C. (2013),
1331 The 2010 California Research at the Nexus of Air Quality and Climate Change (CalNex) field
1332 study, *J. Geophys. Res.*, 118, 5830–5866.

1333 Schere, K. J. Flemming, R. Vautard, C. Chemel, A. Colette, C. Hogrefe, B. Bessagnet, F. Meleux,
1334 R. Mathur, S. Roselle, R.-M. Hu, R. S. Sokhi, S. T. Rao, S. Galmarini (2012), Trace gas/aerosol
1335 boundary concentrations and their impacts on continental-scale AQMEII modeling domains,
1336 *Atmos. Environ.*, 53, 38-50, doi: 10.1016/j.atmosenv.2011.09.043.

1337 Shindell, D. T., G. Faluvegi, D. M. Koch, G. A. Schmidt, N. Unger, and S. E. Bauer (2009),
1338 Improved attribution of climate forcing to emissions, *Science*, 326, 716–718, doi:
1339 10.1126/science.1174760.

1340 Shindell, D. T., et al. (2013), Radiative forcing in the ACCMIP historical and future climate
1341 simulations, *Atmos. Chem. Phys.*, 13, 2939–2974, doi:10.5194/acp-13-2939-2013.

1342 Simpson, D., Benedictow, A., Berge, H., Bergström, R., Emberson, L. D., Fagerli, H., Flechard,
1343 C. R., Hayman, G. D., Gauss, M., Jonson, J. E., Jenkin, M. E., Nyíri, A., Richter, C., Semeena,
1344 V. S., Tsyro, S., Tuovinen, J.-P., Valdebenito, Á., and Wind, P. (2012), The EMEP MSC-W
1345 chemical transport model – technical description, *Atmos. Chem. Phys.*, 12, 7825–7865,
1346 doi:10.5194/acp-12-7825-2012.

1347 Sindelarova, K., Granier, C., Bouarar, I., Guenther, A., Tilmes, S., Stavrou, T., Müller, J.-F.,
1348 Kuhn, U., Stefani, P., and Knorr, W. (2014), Global data set of biogenic VOC emissions
1349 calculated by the MEGAN model over the last 30 years, *Atmos. Chem. Phys.*, 14, 9317–9341,
1350 doi:10.5194/acp-14-9317-2014.

1351 Skamarock, W. C., J. B. Klemp, J. Dudhia, D. Gill, D. M. Barker, W. Wang, and J. G. Powers
1352 (2008), A description of the Advanced Research WRF version 3 (Available at
1353 www.mmm.ucar.edu/wrf/users/docs/arwv3.pdf).

1354 Smith, K. R., Jerrett, M., and Anderson, H. R. et al. (2009), Public health benefits of strategies to
1355 reduce greenhouse-gas emissions: health implications of short-lived greenhouse pollutants,
1356 *Lancet*, doi: 10.1016/S0140-6736 (09) 61716-5.

1357 Solazzo, E. R. Bianconi, R. Vautard, K. W. Appel, M. D. Moran, C. Hogrefe, B. Bessagnet, J.
1358 Brandt, J. H. Christensen, C. Chemel, I. Coll, H. D. van der Gon, J. Ferreira, R. Forkel, X. V.
1359 Francis, G. Grell, P. Grossi, A. B. Hansen, A. Jeričević, L. Kraljević, A. I. Miranda, U.
1360 Nopmongcol, G. Pirovano, M. Prank, A. Riccio, K. N. Sartelet, M. Schaap, J. D. Silver, R. S.
1361 Sokhi, J. Vira, J. Werhahn, R. Wolke, G. Yarwood, J. Zhang, S.T. Rao, S. Galmarini (2012),
1362 Model evaluation and ensemble modelling of surface-level ozone in Europe and North
1363 America in the context of AQMEII, *Atmos. Environ.*, 53, 60-74, , doi:
1364 10.1016/j.atmosenv.2012.01.003.

1365 Søvde, O. A., Prather, M. J., Isaksen, I. S. A., Berntsen, T. K., Stordal, F., Zhu, X., Holmes, C. D.,
1366 and Hsu, J. (2012), The chemical transport model Oslo CTM3, *Geosci. Model Dev.*, 5, 1441–
1367 1469, doi:10.5194/gmd-5-1441-2012.

1368 Sudo, K., M. Takahashi, J. Kurokawa, and H. Akimoto (2002), Chaser: A global chemical model
1369 of the troposphere, 1. Model description, *J. Geophys. Res.*, 107(D17), 4339,
1370 doi:10.1029/2001JD001113.

1371 Stevenson, D. S., et al. (2006), Multimodel ensemble simulations of present-day and near-future
1372 tropospheric ozone, *J. Geophys. Res.*, 111, D08301, doi:10.1029/2005JD006338.

1373 Stevenson, D. S., et al. (2013), Tropospheric ozone changes, radiative forcing and attribution to
1374 emissions in the Atmospheric Chemistry and Climate Model Intercomparison Project
1375 (ACCMIP), *Atmos. Chem. Phys.*, 13, 3063–3085, doi:10.5194/acp-13-3063-2013.

1376 Susaya, J., Kim, K.-H., Shon, Z.-H., Brown R. J. (2013), Demonstration of long-term increases in
1377 tropospheric O₃ levels: Causes and potential impacts, *Chemosphere*, 92, 1520–1528.

1378 Task Force on Hemispheric Transport of Air Pollution (HTAP) (2010), 2010 Final Assessment
1379 report, Part A: Ozone and particulate matter,
1380 [http://www.htap.org/activities/2010_Final_Report/HTAP%202010%20Part%20A%2011040](http://www.htap.org/activities/2010_Final_Report/HTAP%202010%20Part%20A%20110407.pdf)
1381 [7.pdf](http://www.htap.org/activities/2010_Final_Report/HTAP%202010%20Part%20A%20110407.pdf).

1382 Tilmes, S., Lamarque, J.-F., Emmons, L. K., Kinnison, D. E., Marsh, D., Garcia, R. R., Smith, A.
1383 K., Neely, R. R., Conley, A., Vitt, F., Val Martin, M., Tanimoto, H., Simpson, I., Blake, D. R.,
1384 and Blake, N. (2016), Representation of the Community Earth System Model (CESM1)
1385 CAM4-chem within the Chemistry- Climate Model Initiative (CCMI), *Geosci. Model Dev.*, 9,
1386 1853– 1890, doi:10.5194/gmd-9-1853-2016.

1387 Travis, K. R., Jacob, D. J., Fisher, J. A., Kim, P. S., Marais, E. A., Zhu, L., Yu, K., Miller, C. C.,
1388 Yantosca, R. M., Sulprizio, M. P., Thompson, A. M., Wennberg, P. O., Crounse, J. D., St.
1389 Clair, J. M., Cohen, R. C., Laughner, J. L., Dibb, J. E., Hall, S. R., Ullmann, K., Wolfe, G. M.,
1390 Pollack, I. B., Peischl, J., Neuman, J. A., and Zhou, X. (2016), Why do models overestimate
1391 surface ozone in the Southeast United States?, *Atmos. Chem. Phys.*, 16, 13561-13577,
1392 doi:10.5194/acp-16-13561-2016.

1393 United Nations Environment Programme and World Meteorological Organization (2011),
1394 Integrated Assessment of Black Carbon and Tropospheric Ozone: Summary for Decision
1395 Makers, http://www.unep.org/dewa/Portals/67/pdf/Black_Carbon.pdf.

1396 US EPA (2016a), Implementation of the 2015 Primary Ozone NAAQS: Issues Associated with
1397 Background Ozone White Paper for Discussion,
1398 <https://www.epa.gov/sites/production/files/2016-03/documents/whitepaper-bgo3-final.pdf>.

1399 US EPA (2016b), High level summary of background ozone workshop,
1400 [https://www.epa.gov/sites/production/files/2016-03/documents/bgo3-high-level-](https://www.epa.gov/sites/production/files/2016-03/documents/bgo3-high-level-summary.pdf)
1401 [summary.pdf](https://www.epa.gov/sites/production/files/2016-03/documents/bgo3-high-level-summary.pdf).

1402 van der Werf, G. R., Randerson, J. T., Giglio, L., Collatz, G. J., Mu, M., Kasibhatla, P. S., Morton,
1403 D. C., DeFries, R. S., Jin, Y., and van Leeuwen, T. T. (2010), Global fire emissions and the
1404 contribution of deforestation, savanna, forest, agricultural, and peat fires (1997–2009), *Atmos.*
1405 *Chem. Phys.*, 10, 11707-11735, doi:10.5194/acp-10-11707-2010.

1406 van Noije, T. P. C., Eskes, H. J., Dentener, F. J., Stevenson, D. S., Ellingsen, K., Schultz, M. G.,
1407 Wild, O., Amann, M., Atherton, C. S., Bergmann, D. J., Bey, I., Boersma, K. F., Butler, T.,
1408 Cofala, J., Drevet, J., Fiore, A. M., Gauss, M., Hauglustaine, D. A., Horowitz, L. W., Isaksen,
1409 I. S. A., Krol, M. C., Lamarque, J.-F., Lawrence, M. G., Martin, R. V., Montanaro, V., Müller,
1410 J.-F., Pitari, G., Prather, M. J., Pyle, J. A., Richter, A., Rodriguez, J. M., Savage, N. H., Strahan,
1411 S. E., Sudo, K., Szopa, S., and van Roozendaal, M. (2006), Multi-model ensemble simulations
1412 of tropospheric NO₂ compared with GOME retrievals for the year 2000, *Atmos. Chem. Phys.*,
1413 6, 2943-2979, doi:10.5194/acp-6-2943-2006.

1414 Verstraeten, W. W., K. F. Boersma, J. Zörner, M. A. F. Allaart, K. W. Bowman, and J. R. Worden
1415 (2013), Validation of six years of TES tropospheric ozone retrievals with ozonesonde
1416 measurements: Implications for spatial patterns and temporal stability in the bias, *Atmos. Meas.*
1417 *Tech.*, 6, 1413–1423.

1418 Verstraeten, W.W., J. L. Neu, J. E. Williams, K. W. Bowman, J. R. Worden, and K. F. Boersma
1419 (2015), Rapid increases in tropospheric ozone production and export from China, *Nature*
1420 *Geoscience*, 8, 690–695, doi:10.1038/ngeo2493.

1421 Wang, H., D. J. Jacob, P. L. Sager, D. G. Streets, R. J. Park, A. B. Gilliland, and A. van Donkelaar
1422 (2009), Surface ozone background in the United States: Canadian and Mexican pollution
1423 influences, *Atmos. Environ.*, 43(6), 1310–1319, doi:10.1016/j.atmosenv.2008.11.036.

1424 Wang, Y., Konopka, P., Liu, Y., Chen, H., Müller, R., Plöger, F., Riese, M., Cai, Z., and Lü, D.
1425 (2012), Tropospheric ozone trend over Beijing from 2002–2010: ozonesonde measurements
1426 and modeling analysis, *Atmos. Chem. Phys.*, 12, 8389-8399, doi:10.5194/acp-12-8389-2012.

1427 Warneke, C., J. A. deGouw, J. S. Holloway, J. Peischl, T. B. Ryerson, E. Atlas, D. Blake, M.
1428 Trainer, and D. D. Parrish (2012), Multiyear trends in volatile organic compounds in Los
1429 Angeles, California: Five decades of decreasing emissions, *J. Geophys. Res.*, 117, D00V17,
1430 doi:10.1029/2012JD017899.

1431 Warner, J. X., McCourt Comer, M., Barnet, C. D., McMillan, W. W., Wolf, W., Maddy, E., and
1432 Sachse, G. (2007), A comparison of satellite tropospheric carbon monoxide measurements
1433 from AIRS and MOPITT during INTEX-A, *J. Geophys. Res.*, 112, D12S17,
1434 doi:10.1029/2006JD007925, 2007.

1435 Wiedinmyer, C., Akagi, S. K., Yokelson, R. J., Emmons, L. K., Al-Saadi, J. A., Orlando, J. J., and
1436 Soja, A. J. (2011), The Fire INventory from NCAR (FINN): a high resolution global model to
1437 estimate the emissions from open burning, *Geosci. Model Dev.*, 4, 625-641, doi:10.5194/gmd-
1438 4-625-2011.

1439 Wigder, N.L., Jaffe, D.A., Herron-Thorpe, F.L., and Vaughan, J.K. (2013), Influence of daily
1440 variations in baseline ozone on urban air quality in the United States Pacific Northwest, *J.*
1441 *Geophys. Res.*, 118, 3343–3354, doi: 10.1029/2012JD018738.

1442 Wild, O., Fiore, A. M., Shindell, D. T., Doherty, R. M., Collins, W. J., Dentener, F. J., Schultz, M.
1443 G., Gong, S., MacKenzie, I. A., Zeng, G., Hess, P., Duncan, B. N., Bergmann, D. J., Szopa,
1444 S., Jonson, J. E., Keating, T. J., and Zuber, A. (2012), Modelling future changes in surface
1445 ozone: a parameterized approach, *Atmos. Chem. Phys.*, 12, 2037-2054, doi:10.5194/acp-12-
1446 2037-2012.

1447 Wu, S., B. N. Duncan, D. J. Jacob, A. M. Fiore, and O. Wild (2009), Chemical nonlinearities in
1448 relating intercontinental ozone pollution to anthropogenic emissions, *Geophys. Res. Lett.*, 36,
1449 L05806, doi:10.1029/2008GL036607.

1450 Yarwood, G., Rao, S., Yocke, M., and Whitten, G. (2005), Updates to the carbon bond chemical
1451 mechanism: CB05. Final report to the US EPA, EPA Report Number: RT-0400675.

1452 Zhang, L., Jacob, D. J., Boersma, K. F., Jaffe, D. A., Olson, J. R., Bowman, K. W., Worden, J. R.,
1453 Thompson, A. M., Avery, M. A., Cohen, R. C., Dibb, J. E., Flock, F. M., Fuelberg, H. E.,
1454 Huey, L. G., McMillan, W. W., Singh, H. B., and Weinheimer, A. J. (2008), Transpacific
1455 transport of ozone pollution and the effect of recent Asian emission increases on air quality in
1456 North America: an integrated analysis using satellite, aircraft, ozonesonde, and surface
1457 observations, *Atmos. Chem. Phys.*, 8, 6117-6136, doi:10.5194/acp-8-6117-2008.

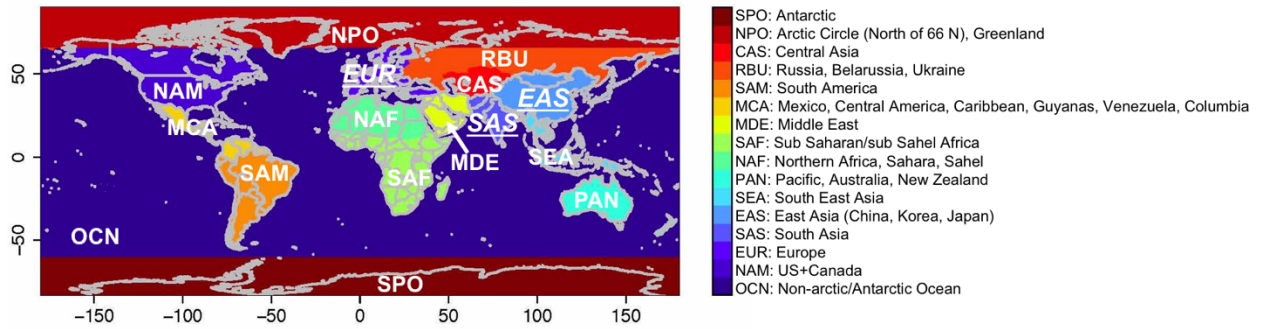
1458 Zhang, L., Jacob, D. J., Kopacz, M., Henze, D. K., Singh, K., and Jaffe, D. A. (2009),
1459 Intercontinental source attribution of ozone pollution at western U.S. sites using an adjoint
1460 method, *Geophys. Res. Lett.*, 36, L11810, doi: 10.1029/2009GL037950.

1461 Zhang, L., D. J. Jacob, N. V. Downey, D. A. Wood, D. Blewitt, C. C. Carouge, A. van Donkelaar,
1462 D. B. A. Jones, L. T. Murray, and Y. Wang (2011), Improved estimate of the policy-relevant
1463 background ozone in the United States using the GEOS-Chem global model with $1/2^\circ \times 2/3^\circ$
1464 horizontal resolution over North America, *Atmos. Environ.*, 45, 6769–6776, doi:
1465 10.1016/j.atmosenv.2011.07.054.

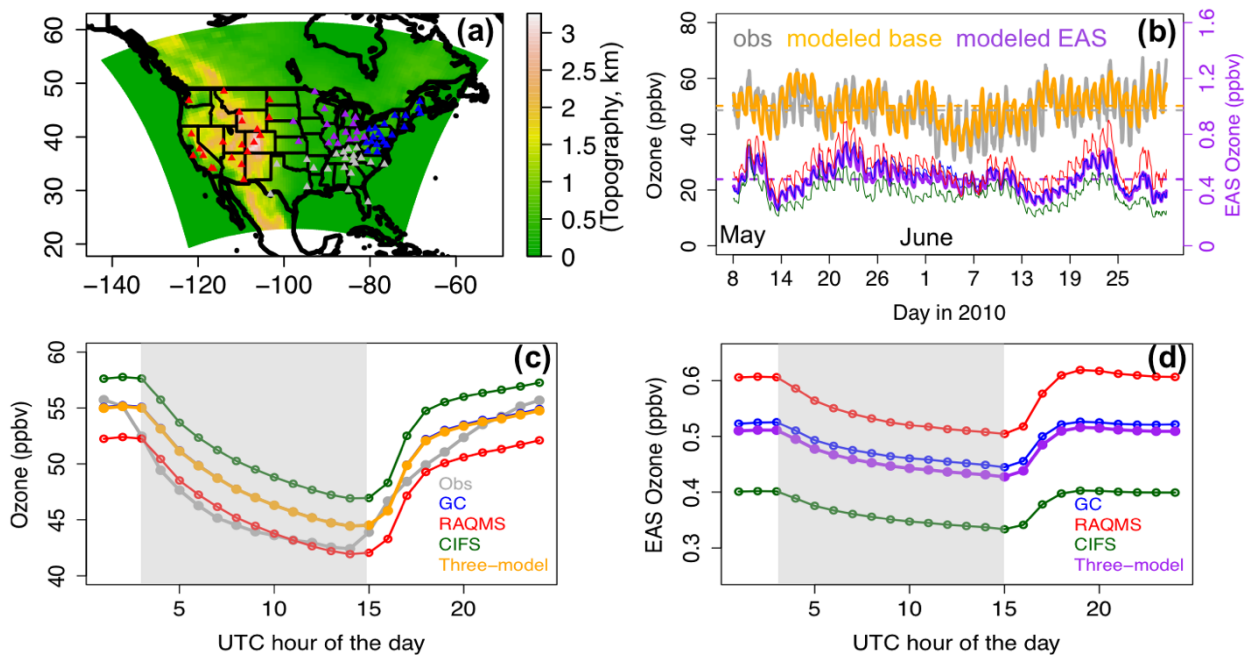
1466 Zhang, Q., Yuan, B., Shao, M., Wang, X., Lu, S., Lu, K., Wang, M., Chen, L., Chang, C.-C., and
1467 Liu, S. C. (2014), Variations of ground-level O₃ and its precursors in Beijing in summertime
1468 between 2005 and 2011, *Atmos. Chem. Phys.*, 14, 6089-6101, doi:10.5194/acp-14-6089-2014.

1469 Zhang, Y., Y. Chen, G. Sarwar, and K. Schere (2012), Impact of gas-phase mechanisms on
1470 Weather Research Forecasting Model with Chemistry (WRF/Chem) predictions: Mechanism
1471 implementation and comparative evaluation, *J. Geophys. Res.*, 117, D01301,
1472 doi:10.1029/2011JD015775.

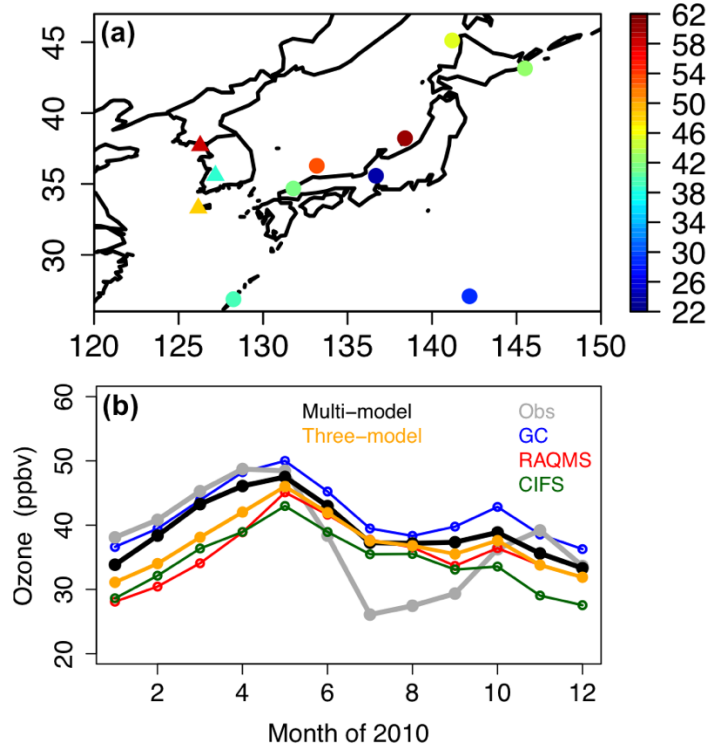
1473 Zoogman, P., X. Liu, R.M. Suleiman, W.F. Pennington, D.E. Flittner, J.A. Al-Saadi, B.B. Hilton,
1474 D.K. Nicks, M.J. Newchurch, J.L. Carr, S.J. Janz, M.R. Andraschko, A. Arola, B.D. Baker,
1475 B.P. Canova, C. Chan Miller, R.C. Cohen, J.E. Davis, M.E. Dussault, D.P. Edwards, J.
1476 Fishman, A. Ghulam, G. González Abad, M. Grutter, J.R. Herman, J. Houck, D.J. Jacob, J.
1477 Joiner, B.J. Kerridge, J. Kim, N.A. Krotkov, L. Lamsal, C. Li, A. Lindfors, R.V. Martin, C.T.
1478 McElroy, C. McLinden, V. Natraj, D.O. Neil, C.R. Nowlan, E.J. O'Sullivan, P.I. Palmer, R.B.
1479 Pierce, M.R. Pippin, A. Saiz-Lopez, R.J.D. Spurr, J.J. Szykman, O. Torres, J.P. Veefkind, B.
1480 Veihelmann, H. Wang, J. Wang, and K. Chance (2017), Tropospheric emissions: Monitoring
1481 of pollution (TEMPO), *Journal of Quantitative Spectroscopy and Radiative Transfer*, 186, 17-
1482 39, doi: 10.1016/j.jqsrt.2016.05.008.



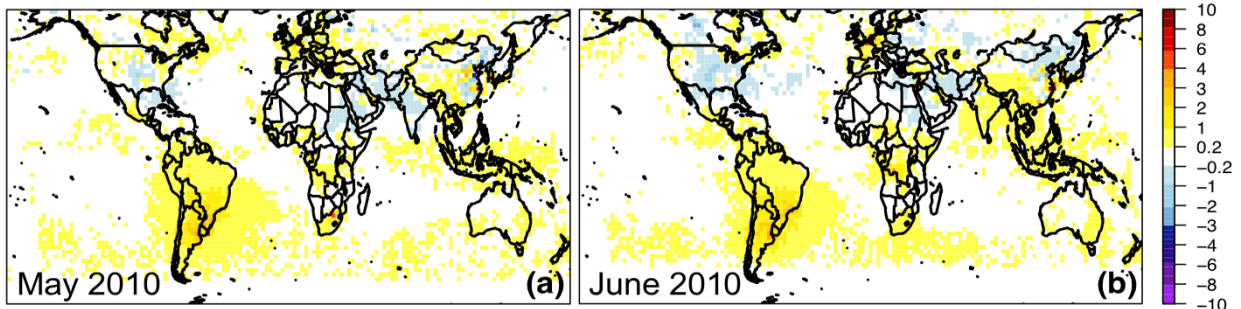
1483
 1484 **Figure 1.** Definitions of the 16 source regions used in HTAP2 SR relationship study (More details
 1485 in Koffi et al., 2016). The map is plotted based on data on a $0.1^\circ \times 0.1^\circ$ resolution grid. We focus
 1486 in this study on the impact of anthropogenic pollution from selected non-North American source
 1487 regions (i.e., EAS, SAS, and EUR), whose names are underlined and in italic.
 1488



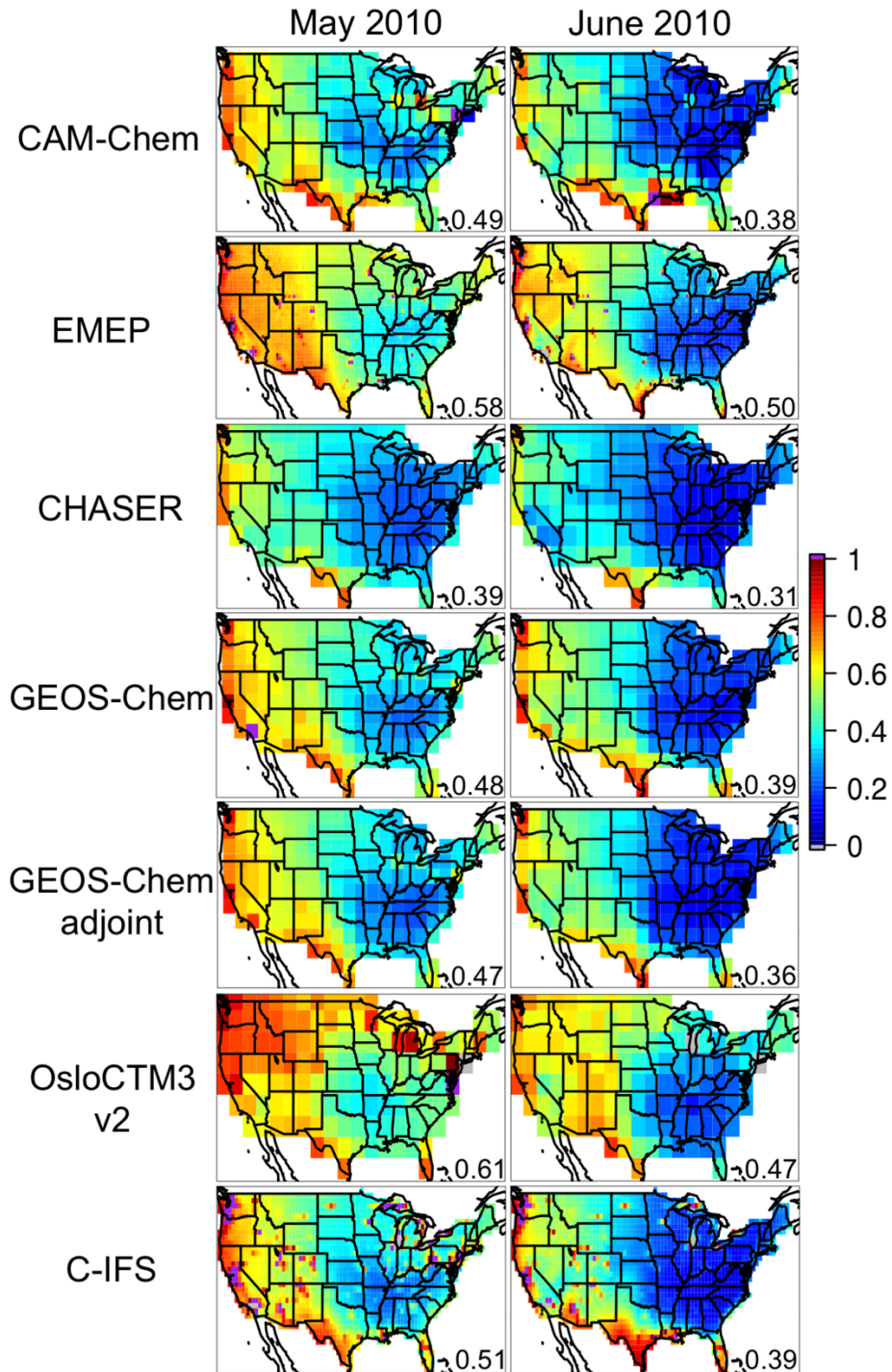
1489
 1490 **Figure 2.** (a) The 60 km STEM NAM domain, colored by the model topography. The CASTNET
 1491 sites used in the STEM base O₃ evaluation are marked as triangles in different colors that identify
 1492 the subregions they belong to (red: western US; grey: southern US; purple: Midwest; blue:
 1493 northeastern US). (b) Evaluation of the STEM modeled (averaged from the three base simulations
 1494 using the GEOS-Chem, ECMWF C-IFS, and RAQMS base runs as the chemical boundary
 1495 conditions) hourly O₃ at the western US (i.e., EPA regions 8, 9, and 10) CASTNET sites.
 1496 Observations, modeled base O₃ and the modeled R(O₃, EAS, 20%) are in grey, orange, and purple
 1497 lines, respectively. The horizontal dashed lines indicate the period mean values. The R(O₃, EAS,
 1498 20%) values from STEM calculations using three different chemical boundary conditions
 1499 are shown separately in thin lines (blue: GEOS-Chem; red: RAQMS; green: C-IFS). The period-mean
 1500 diurnal variability of the STEM modeled (c) base and (d) R(O₃, EAS, 20%) at the western US
 1501 CASTNET sites. The STEM calculations using three different chemical boundary conditions are
 1502 shown separately as well as averagely. Light grey-shaded areas indicate the local standard
 1503 nighttime (from 6/7 pm to 7/8 am).



1504 **Figure 3.** (a) May-June 2010 period mean surface O₃ observations in ppbv at eight Japanese (filled
 1505 circles) and three Korean (filled triangles) EANET sites. (b) Observed and modeled monthly-mean
 1506 surface O₃ in 2010 at all eleven EANET sites. The “Multi-model” and “Three-model” in the legend
 1507 indicate the mean values of all eight global models and only of the three boundary condition
 1508 models, respectively.
 1509
 1510

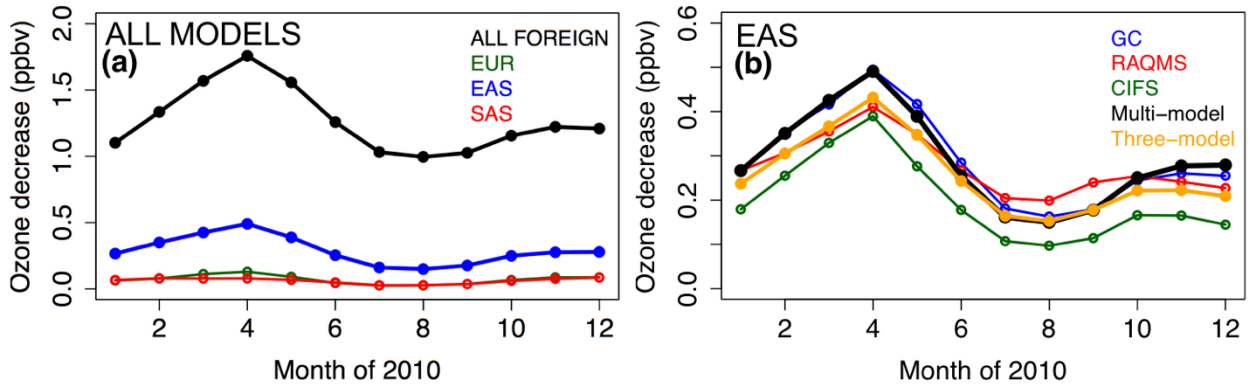


1511 **Figure 4.** Evaluation of the GEOS-Chem adjoint base NO₂ product (recorded at near the satellite
 1512 overpassing time) with the OMI NO₂ columns. The differences between OMI and GEOS-Chem
 1513 (OMI-modeled) tropospheric NO₂ columns ($\times 10^{15}$ molec./cm²) are shown for (a) May and (b) June
 1514 2010. Details of the comparison are included in Section 2.3.2.
 1515
 1516

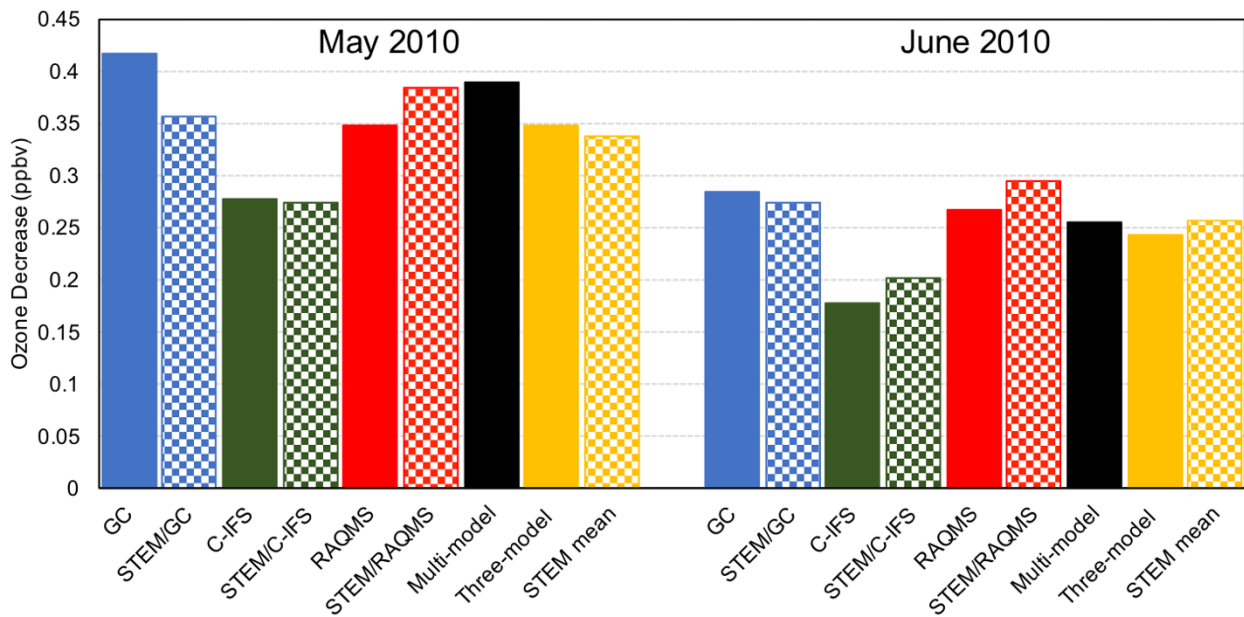


1517
 1518
 1519
 1520
 1521
 1522
 1523
 1524

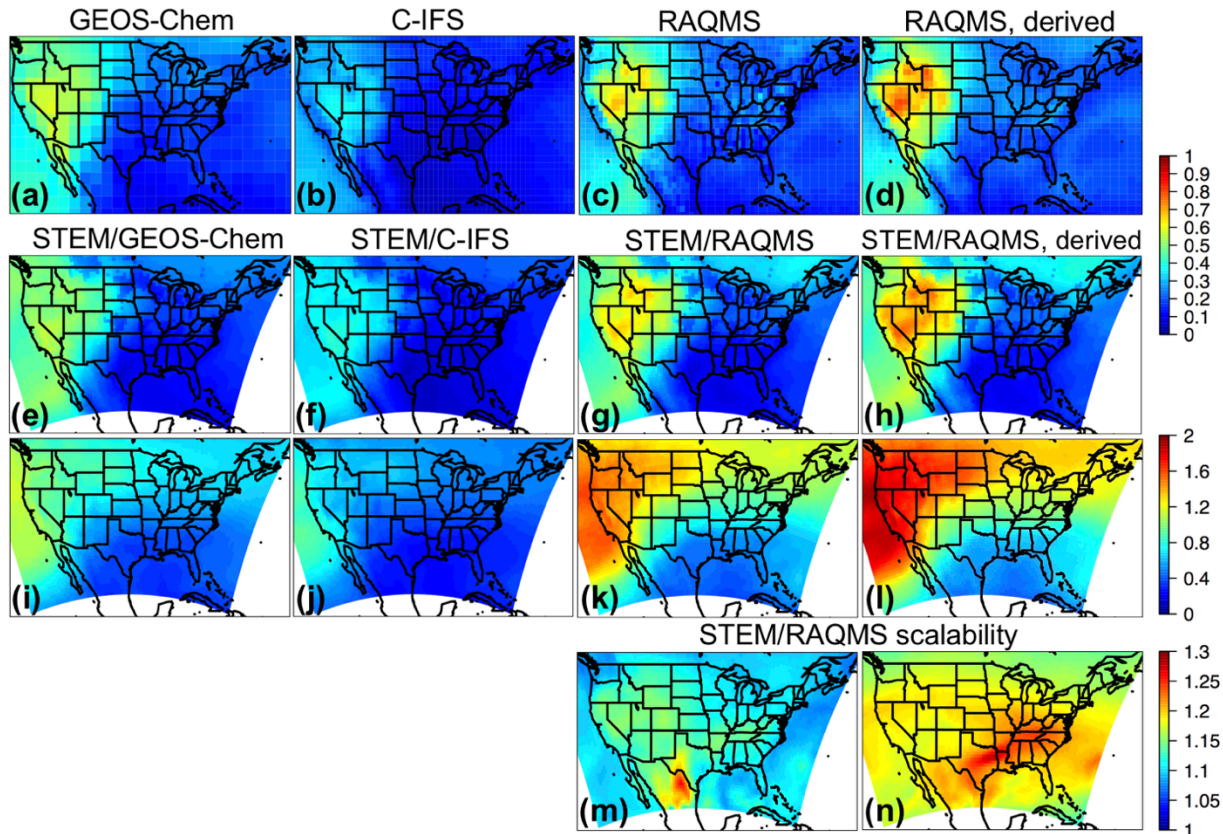
Figure 5. The RERER maps in May (left) and June (right) 2010 over the continental US, calculated based on the monthly mean O_3 from multiple global models' base and emission sensitivity simulations. The RERER metric (unitless) was defined in eq. (2) in the text. Values larger than 1 and smaller than 0 are shown in purple and grey, respectively. The US (including continental US as well as Hawaii which is not shown in the plots) mean values are indicated for each panel at the lower right corner. All models show declining RERER values from May to June, and the 7-model mean RERER values for May and June 2010 are ~ 0.5 and ~ 0.4 , respectively.



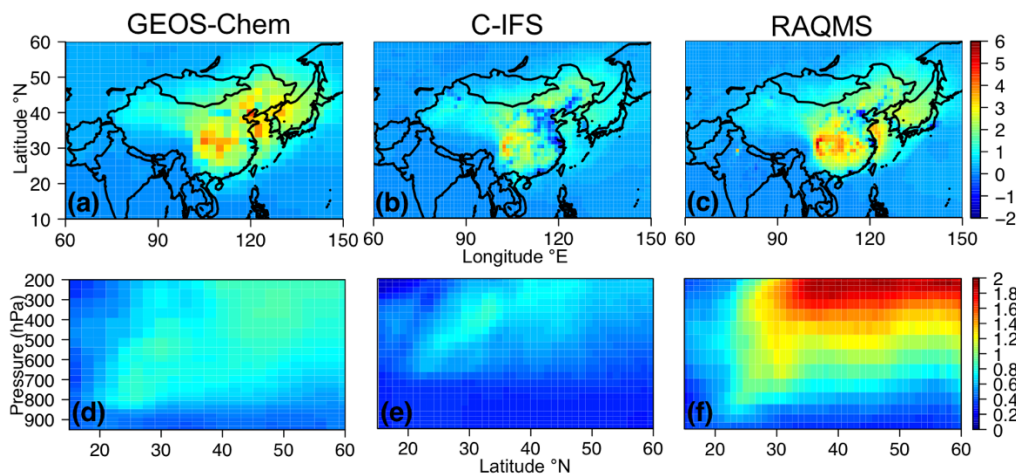
1525
 1526 **Figure 6. (a)** North American (130-65°W; 20-50°N) mean O₃ sensitivity to 20% anthropogenic
 1527 emission reductions in various non-North American regions, averaged from multiple (six-eight,
 1528 see details in text) global models. **(b)** North American surface R(O₃, EAS, 20%) values, as
 1529 as estimated by single (the three STEM boundary condition models) or multi- global model means.
 1530 The “Multi-model” and “Three-model” in the legend indicate the mean sensitivities of all eight
 1531 global models and only of the three boundary condition models, respectively.
 1532



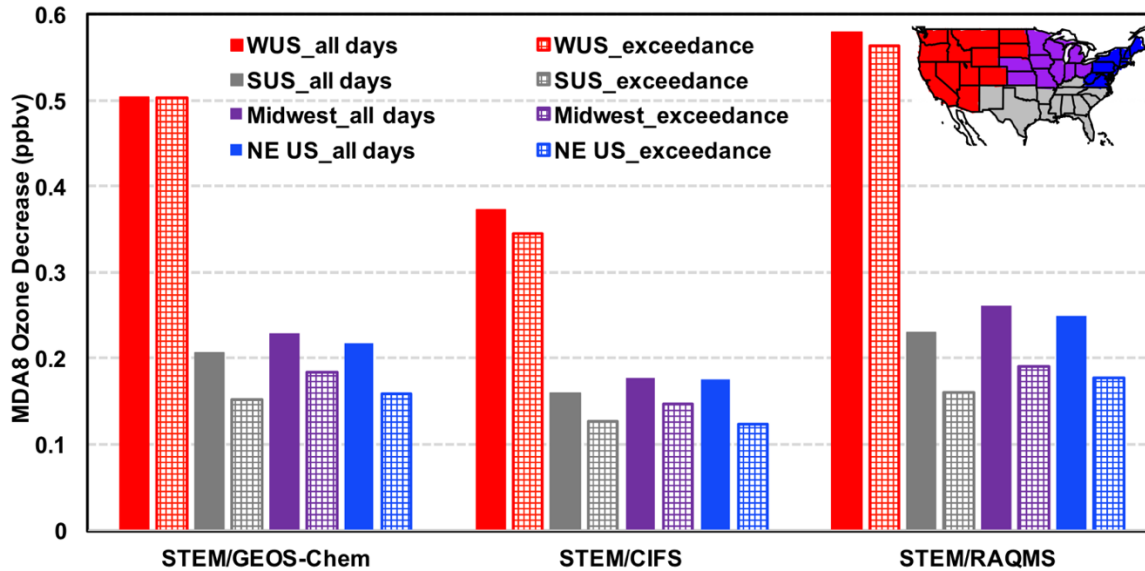
1533
 1534 **Figure 7.** Monthly-mean North American (130-65°W; 20-50°N) surface R(O₃, EAS, 20%) values
 1535 from multiple global and regional model simulations for May (left) and June (right) 2010. STEM
 1536 model mean values were calculated from its hourly output from 8 May and on. The “Multi-model”
 1537 and “Three-model” in the legend indicate the mean sensitivities of all eight global models and only
 1538 of the three boundary condition models, respectively.



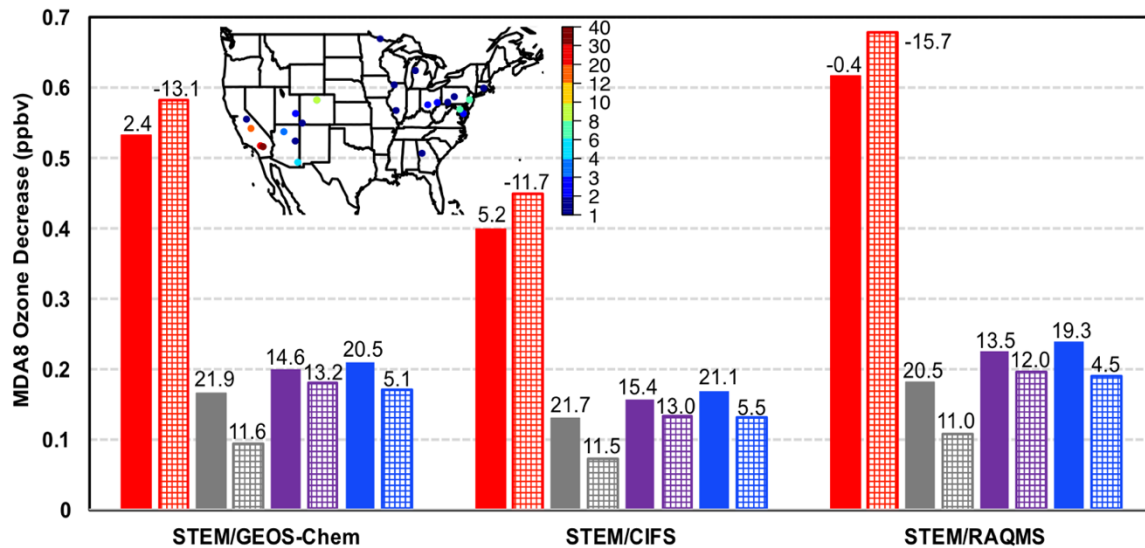
1539
 1540 **Figure 8.** The monthly-mean $R(\text{O}_3, \text{EAS}, 20\%)$ in June 2010 for: (a-d) surface O_3 (ppbv) from the
 1541 three boundary condition models, (e-h) STEM surface O_3 (ppbv), and (i-l) STEM column O_3
 1542 ($\times 10^{16}$ molecules/ cm^2). $R(\text{O}_3, \text{EAS}, 20\%)$ values from the simulations associated with GEOS-
 1543 Chem, ECMWF C-IFS, and RAQMS are shown in (a;e;i), (b;f;j) and (c;g;k), respectively. (d;h;l)
 1544 show 1/5 of the $R(\text{O}_3, \text{EAS}, 100\%)$ from the simulations related to RAQMS. STEM/RAQMS-
 1545 based “Scalability” S_{O_3} (eq. (3)) values over the NAM are shown for (m) surface and (n) column
 1546 O_3 .



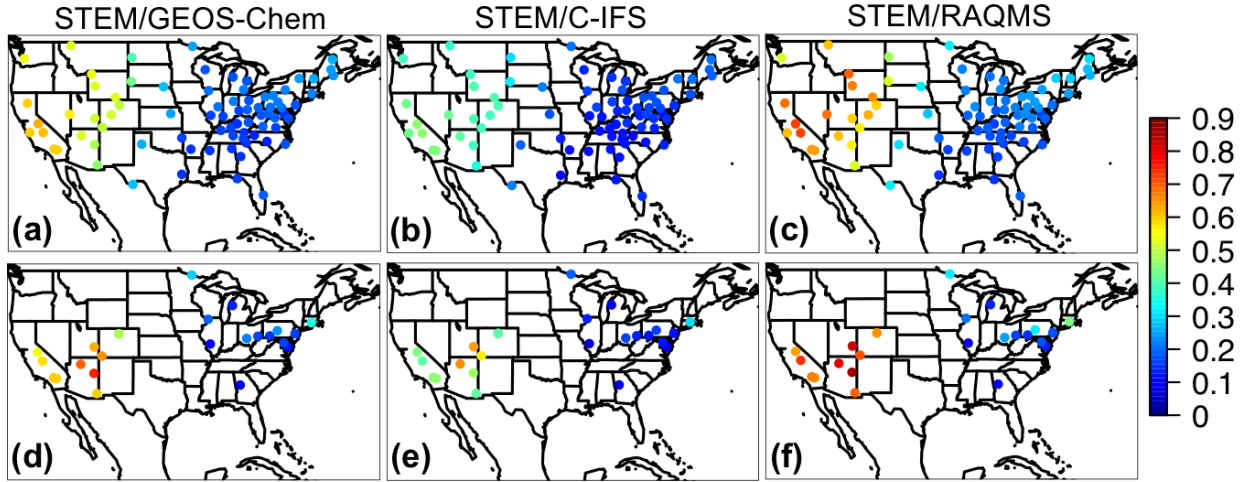
1547
 1548 **Figure 9.** The monthly-mean $R(\text{O}_3, \text{EAS}, 20\%)$ in ppbv in June 2010 from the three boundary
 1549 condition models at the source and near the receptor regions: (a-c) surface O_3 in the East Asia; and
 1550 (d) O_x (GEOS-Chem) or (e-f) O_3 (ECMWF C-IFS and RAQMS) along the cross section of 135°W
 1551 (near the west boundary of the STEM model domain as defined in Figure 2a).



1552
 1553 **Figure 10.** STEM R(MDA8, EAS, 20%) for May-June 2010 in four US subregions (defined in the
 1554 inset panel, also consistent with the definitions in Figures 2/S4 and Tables 2-3), averaged on all
 1555 days (bars with solid fill) and only on the days when the simulated total MDA8 O₃ concentrations
 1556 were over 70 ppbv (bars with grid pattern fill). The results from the STEM runs using GEOS-
 1557 Chem, ECMWF C-IFS and RAQMS boundary conditions are shown separately.
 1558

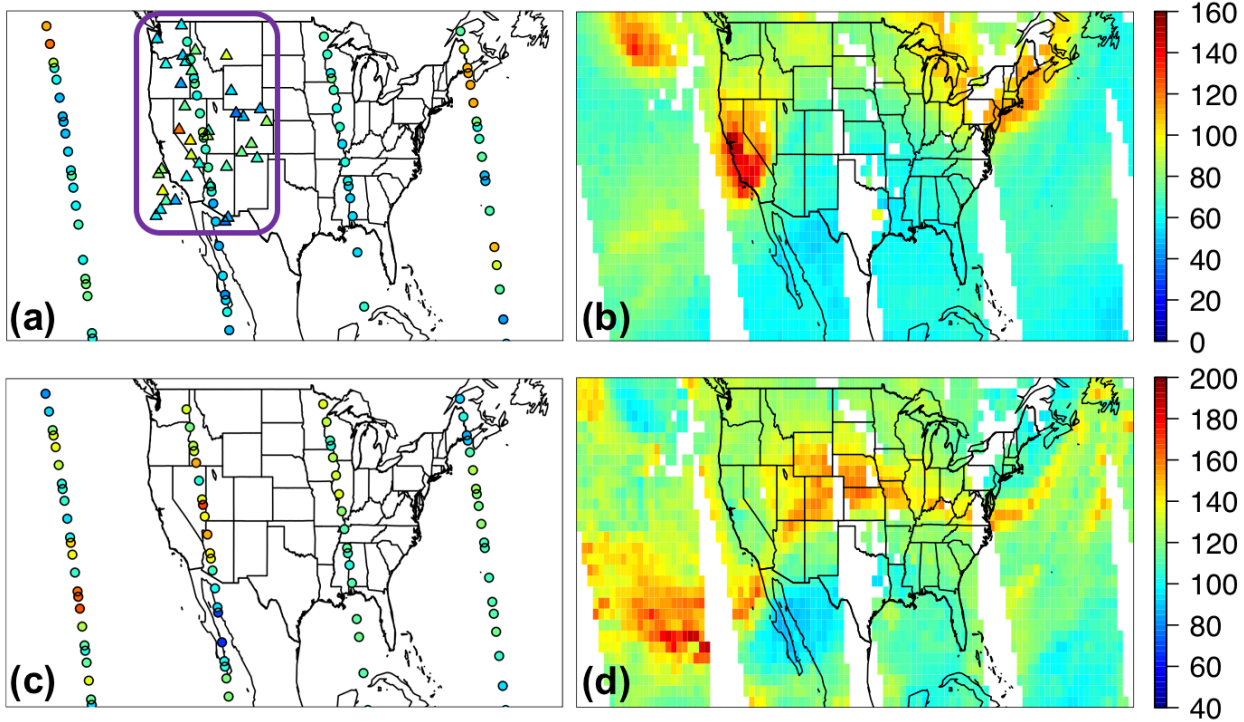


1559
 1560 **Figure 11.** STEM R(MDA8, EAS, 20%) for May-June 2010 at the CASTNET sites in four US
 1561 subregions (same definition as in Figure 10 inset), averaged on all days (bars with solid fill) and
 1562 only on the days when the observed MDA8 O₃ concentrations were over 70 ppbv (bars with grid
 1563 pattern fill). The results from the STEM runs using GEOS-Chem, ECMWF C-IFS and RAQMS
 1564 boundary conditions are shown separately. Biases for the corresponding model base runs are
 1565 shown above the bar plots. Inset shows at various CASTNET sites the number of days when the
 1566 observed MDA8 O₃ concentrations were over 70 ppbv.
 1567



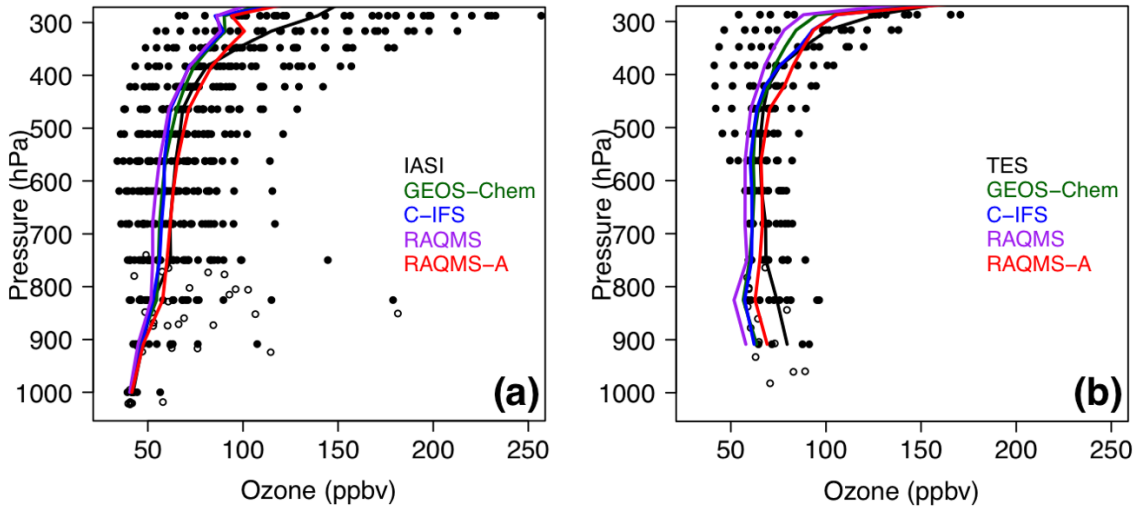
1568
1569
1570
1571
1572
1573

Figure 12. STEM R(MDA8, EAS, 20%) in ppbv for May-June 2010 at the CASTNET sites on (a-c) all days and (d-f) the days when the observed MDA8 O₃ concentrations were over 70 ppbv. The results from the STEM runs using (a;d) GEOS-Chem, (b;e) ECMWF C-IFS and (c;f) RAQMS boundary conditions are shown separately.

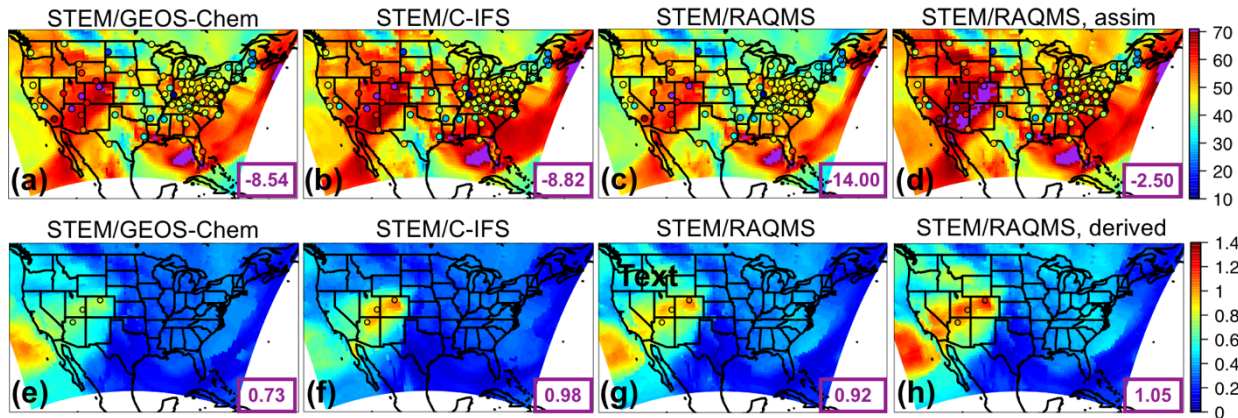


1574
1575
1576
1577
1578
1579

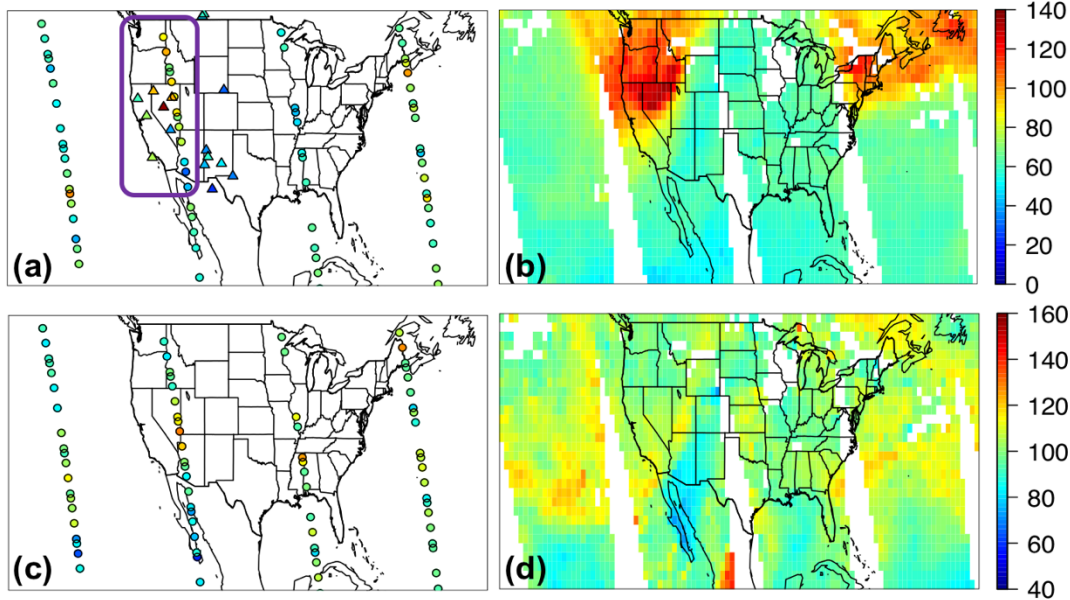
Figure 13. Case study of 9 May 2010: (a-b) Ozone (ppbv) and (c-d) CO (ppbv) at ~500 hPa from the L2 (a;c) TES retrievals (circles) and (b;d) L3 AIRS products at early afternoon local time. The L2 IASI O₃ (ppbv) at ~500 hPa retrieved using the TES algorithm (details in Section 2.3.2) at the mid-morning local times is shown on panel (b) as triangles. The O₃ profiles within the purple box in panel (a) were used in the model evaluation shown in Figure 14.



1580
 1581 **Figure 14.** Case study of 9 May 2010: The comparisons between (a) IASI and (b) TES O₃ in the
 1582 western US with the simulated O₃ in the STEM runs using the GEOS-Chem (green), C-IFS (blue),
 1583 RAQMS (purple), and assimilated RAQMS (red) boundary conditions. The O₃ profiles within the
 1584 purple box in Figure 10a were used in the evaluation. Observation operators were applied in the
 1585 comparisons (details in Section 2.3.2). Solid and open dots are TES/IASI data at the TES retrieval
 1586 reporting levels and at the variable surface pressure levels, respectively. Solid lines are median O₃
 1587 profiles from the satellite observations and the different STEM simulations, calculated only on the
 1588 TES retrieval reporting levels.
 1589

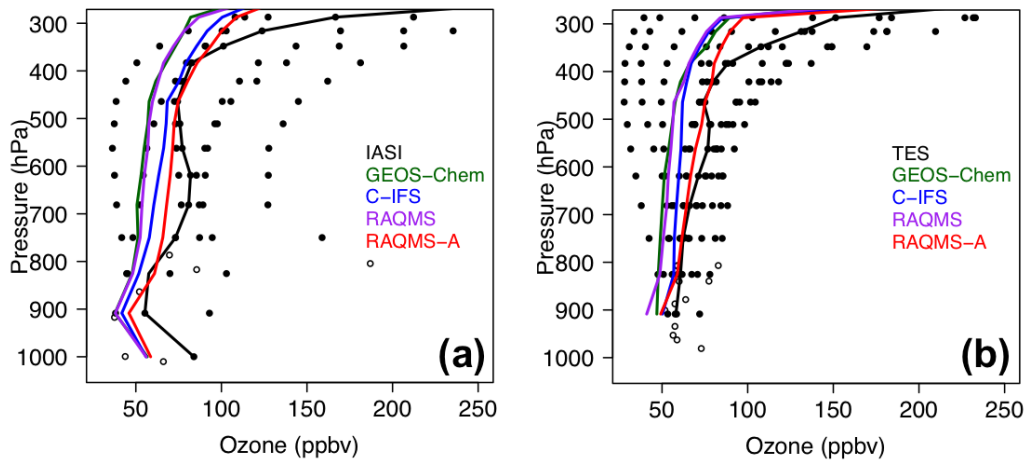


1590
 1591 **Figure 15.** Case study of 9 May 2010: (a-d) Surface MDA8 total O₃ and (e-h) surface R(MDA8,
 1592 EAS, 20%) from the STEM simulations using the (a;e) GEOS-Chem, (b;f) ECMWF C-IFS, and
 1593 (c;g) RAQMS free run as the boundary conditions. (d) Surface MDA8 total O₃ in a STEM base
 1594 simulation using the RAQMS assimilation run as the boundary conditions. CASTNET
 1595 observations are overlaid in filled circles in panels (a-d). (h) 1/5 of the surface R(MDA8, EAS,
 1596 100%) from STEM/RAQMS simulations. The conditions at ~400-500 hPa are shown in Figure S5.
 1597 Purple numbers at the lower right corners of (a-d) and (e-h) are mean model biases and mean
 1598 R(MDA8, EAS, 20%) values in ppbv at the three mountain sites (Grand Canyon NP, AZ;
 1599 Canyonlands NP, UT; and Rocky Mountain NP, CO) where O₃ exceedances were observed on this
 1600 day. The locations of these sites are shown in panel (e-h) as open circles.
 1601



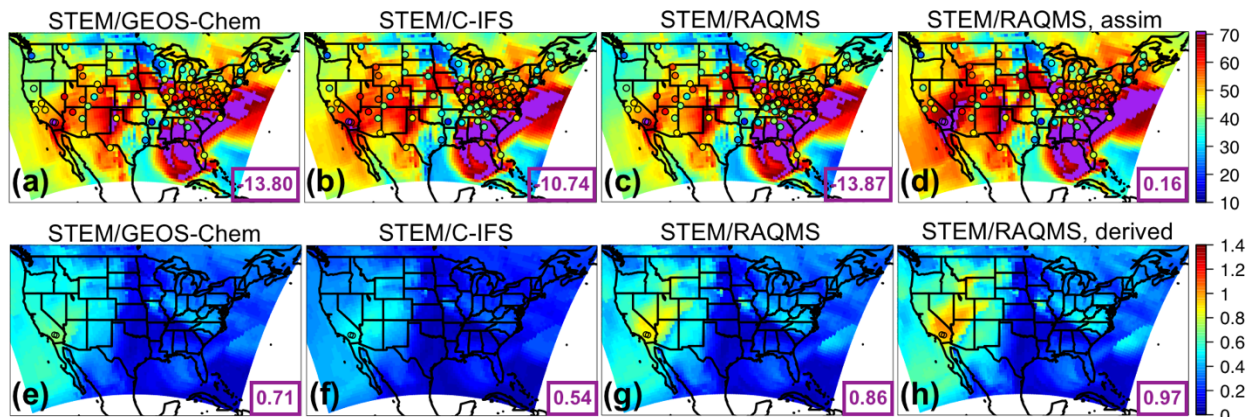
1602
1603
1604

Figure 16. Same as Figure 13, but for a case study of 10 June 2010.



1605
1606
1607

Figure 17. Same as Figure 14, but for a case study of 10 June 2010.



1608
1609
1610

Figure 18. Same as Figure 15, but for a case study of 10 June 2010. The CASTNET sites with O_3 exceedances on this day are Converse Station and Joshua Tree NP in southern California.

1611 **Table 1a.** HTAP2 base and sensitivity simulations by various global models. The STEM boundary
 1612 condition models are highlighted in bold.

Global model, Resolution: lon×lat×vertical layer, (References)	BASE	EASALL (-20%)	EASALL (-100%)	GLOALL (-20%)	NAMALL (-20%)	EURALL (-20%)	SASALL (-20%)
CAM-Chem, 2.5°×1.9°×56 (Tilmes et al., 2016)	✓	✓		✓	✓	✓	✓
CHASER T42, ~2.8°×2.8°×32 (Sudo et al., 2002)	✓	✓		✓	✓	✓	✓
EMEP rv48, 0.5°×0.5°×20 (Simpson et al., 2012)	✓	✓		✓	✓	✓	✓
SNU GEOS-Chem v9-01-03, 2.5°×2°×47 (Park et al., 2004; http://iek8wikis.iek.fz-juelich.de/HTAPWiki/WP2.3?action=AttachFile&do=view&target=_README_GEOS-Chem.pdf)	✓	✓		✓	✓		
CU-Boulder GEOS-Chem adjoint v35f, 2.5°×2°×47 (Henze et al., 2007)	✓	✓		✓	✓	✓	✓
RAQMS, 1°×1°×35, free running (Pierce et al., 2007, 2009)	✓	✓	✓				
RAQMS, 1°×1°×35, with satellite assimilation (Pierce et al., 2007, 2009)	✓						
OsloCTM3 v2, ~2.8°×2.8°×60 (Søvde et al., 2012)	✓	✓		✓	✓	✓	✓
ECMWF C-IFS, ~0.7°×0.7°×54/1.125°×1.125°×54, as the STEM chemical boundary conditions (Flemming et al., 2015)	✓	✓		✓	✓	✓	✓

1613 Acronyms:

1614 CAM-Chem: Community Atmosphere Model with Chemistry

1615 C-IFS: Composition-Integrated Forecasting System

1616 ECMWF: European Center for Medium range Weather Forecasting

1617 EMEP: European Monitoring and Evaluation Programme

1618 GEOS-Chem: Goddard Earth Observing System with Chemistry

1619 RAQMS: Realtime Air Quality Modeling System

1620 SNU: Seoul National University

1621 **Table 1b.** STEM regional simulations for HTAP2

Boundary condition model, Resolution: lon×lat×vertical layer	BASE	EASALL (-20%)	EASALL (-100%)
SNU GEOS-Chem v9-01-03, 2.5°×2°×47	✓	✓	
RAQMS, 1°×1°×35, free running	✓	✓	✓
RAQMS, 1°×1°×35, with satellite assimilation	✓		
ECMWF C-IFS, 1.125°×1.125°×54	✓	✓	

1622
1623 **Table 1c.** STEM and its boundary condition models' key inputs and chemical mechanisms, with
1624 references. More details on the models can be found in Table 1a and the text.

Model	Meteorology	Biogenic VOCs; NO _x	Lightning	Biomass Burning	Chemical Mechanism
GEOS- Chem	GEOS-5	MEGAN v2.1 (Guenther et al., 2012); Wang et al., 2009	based on GEOS-5 deep convective cloud top heights and climatological observations (Murray et al., 2012)	GFED v3.0 (van der Werf et al., 2010)	GEOS-Chem standard NO _x -O _x - hydrocarbon-aerosol (http://acmg.seas.harvard.edu/geos/doc/archive/man.v9-01-03/appendix_1.html)
RAQMS	Online (Pierce et al., 2007)				CB-IV (Gery et al., 1989) with adjustments
ECMWF C-IFS	IFS	MEGAN- MACC, (Sindelarova et al., 2014); POET database for 2000 (Granier et al., 2005)	based on IFS convective precipitation (Meijer et al., 2001)	GFAS v1.0 (Kaiser et al., 2012)	CB05 (Yarwood et al., 2005)
STEM	WRF-ARW v3.3.1	WRF- MEGAN v2.1	based on scaled WRF convective precipitation	FINN v1.0 (Wiedinmye r et al., 2011)	SAPRC99 (Carter, 2000)

1625 Acronyms:

1626 CB: Carbon Bond

1627 FINN: Fire INventory from NCAR

1628 GFAS: Global Fire Assimilation System

1629 GFED: Global Fire Emissions Database

1630 IFS: Integrated Forecasting System

1631 MACC: Monitoring Atmospheric Composition and Climate

1632 MEGAN: Model of Emissions of Gases and Aerosols from Nature

1633 POET: Precursors of Ozone and their Effects in the Troposphere

1634 WRF-ARW: Advanced Research Weather Research and Forecasting Model

1635 **Table 2a.** Evaluation of the period mean (1 May-30 June, 2010) multi- global model free
 1636 simulations against the CASTNET observations, only at the sites where 95% of the hourly O₃
 1637 observations are available. Evaluation of the individual models is summarized in Table 2b.

Subregion	US EPA regions contained	Number of sites	Mean bias (ppbv)		RMSE (ppbv)	
			3 BC ^a models	8 global models	3 BC models	8 global models
Western US	8, 9, 10	19	-5.68	-2.52	10.37	7.05
Southern US	4, 6	18	11.61	10.24	13.62	11.96
Midwest	5, 7	13	8.03	7.66	9.16	8.67
Northeast	1, 2, 3	17	9.55	10.63	10.28	11.24
All	1-10	67	5.49	6.22	11.11	9.96

1638 ^aBC: Boundary Conditions

1639
 1640 **Table 2b.** Evaluation of the period mean (May-June 2010) global model free simulations against
 1641 the EANET and CASTNET observations. The STEM boundary condition models are highlighted
 1642 in bold.

Network	Number of sites	RMSE (ppbv)							
		CAM-Chem	EMEP	CHASER	SNU GEOS- Chem	GEOS-Chem adjoint	RAQMS	OsloCTM3 v2	C-IFS
CASTNET	67	13.30	11.61	15.43	15.55	13.48	9.32	11.05	11.00
EANET	11	10.38	9.96	11.39	9.18	11.04	8.60	12.97	10.86

1643
 1644 **Table 2c.** Evaluation of the period mean (May-June 2010) multi- global model free simulations
 1645 against the EANET observations in Japan and Korea. Evaluation of the individual models is
 1646 summarized in Table 2b.

Country	Number of sites	Mean bias (ppbv)		RMSE (ppbv)	
		3 BC ^a models	8 global models	3 BC models	8 global models
Japan	8	0.36	1.01	8.77	9.25
Korea	3	1.14	3.98	8.37	10.51
All	11	0.57	1.82	8.66	9.61

1647 ^aBC: Boundary Conditions

1648 **Table 3a.** Evaluation of the hourly STEM simulated total O₃ (averaged from the three base
 1649 simulations that used the different free-running boundary conditions) against the CASTNET
 1650 surface observations for 8 May-30 June, 2010. The subregional mean R(O₃, EAS, 100%) and its
 1651 correlation coefficient with the observed O₃ are also shown.

Subregion	US EPA regions contained	Number of sites	Mean elevation (km): actual/model	Mean bias (ppbv)	RMSE (ppbv)	Correlation (model base; obs)	Correlation (obs; modeled EAS)	Mean EAS sensitivity (ppbv)
Western US	8, 9, 10	22	1.75/1.71	1.60	4.86	0.76	0.34	0.48
Southern US	4, 6	22	0.38/0.31	20.33	22.13	0.58	0.27	0.15
Midwest	5, 7	16	0.29/0.28	15.64	17.97	0.70	0.15	0.17
Northeast	1, 2, 3	20	0.36/0.26	20.94	24.16	0.47	0.17	0.21
All	1-10	80	0.73/0.68	16.17	18.30	0.66	0.13	0.20

1652 **Table 3b.** Evaluation of the hourly STEM simulated total O₃ (separately for three base simulations
 1653 that used the different free-running boundary conditions) against the CASTNET surface
 1654 observations for 8 May-30 June, 2010.
 1655

Subregion	US EPA regions contained	Number of sites	Mean bias (ppbv)/RMSE (ppbv)/Correlation (model base; obs)		
			SNU GEOS-Chem	C-IFS	RAQMS
Western US	8, 9, 10	22	1.68/4.83/0.77	4.16/6.63/0.70	-1.03/4.81/0.76
Southern US	4, 6	22	21.18/22.94/0.57	20.34/22.07/0.60	19.48/21.45/0.56
Midwest	5, 7	16	15.77/18.17/0.70	16.41/18.46/0.72	14.73/17.35/0.69
Northeast	1, 2, 3	20	21.25/24.36/0.47	21.86/24.80/0.48	19.71/23.40/0.45
All	1-10	80	16.57/18.62/0.66	16.89/18.84/0.67	15.03/17.52/0.64

1656

1657 **Table 4.** The ranges and standard deviations (ppbv, separated by “;”) of R(O₃, *source region*, 20%)
 1658 by 6-8 global models (defined in eq. (1a-d)), summarized by months in 2010. The monthly multi-
 1659 model mean values are shown in Figures 5-6.

Month/ Source region	All Foreign/ Non-NAM (ppbv)	EUR (ppbv)	EAS (ppbv)	SAS (ppbv)
Jan	0.38-1.69; 0.41	0.002-0.12; 0.05	0.02-0.72; 0.24	0.001-0.11; 0.04
Feb	0.92-2.07; 0.37	0.02-0.15; 0.05	0.16-0.91; 0.28	0.02-0.12; 0.04
Mar	1.30-2.37; 0.38	0.07-0.21; 0.06	0.24-1.03; 0.30	0.03-0.12; 0.03
Apr	1.42-2.46; 0.33	0.09-0.23; 0.05	0.33-1.07; 0.28	0.04-0.12; 0.03
May	1.24-1.91; 0.21	0.06-0.17; 0.04	0.24-0.75; 0.19	0.05-0.11; 0.02
Jun	1.03-1.41; 0.13	0.03-0.07; 0.02	0.14-0.39; 0.09	0.04-0.07; 0.01
Jul	0.86-1.18; 0.13	0.02-0.04; 0.01	0.08-0.22; 0.06	0.01-0.04; 0.01
Aug	0.80-1.19; 0.13	0.01-0.04; 0.01	0.07-0.20; 0.05	0.02-0.04; 0.01
Sep	0.85-1.18; 0.13	0.03-0.05; 0.01	0.10-0.25; 0.06	0.02-0.06; 0.01
Oct	0.96-1.31; 0.14	0.04-0.10; 0.02	0.17-0.42; 0.09	0.03-0.08; 0.02
Nov	0.90-1.48; 0.19	0.05-0.15; 0.04	0.17-0.54; 0.14	0.04-0.10; 0.02
Dec	0.73-1.67; 0.29	0.03-0.18; 0.05	0.14-0.66; 0.19	0.04-0.12; 0.03

1660